## General Comment from Anonymous Referee #1

Thank the authors for putting the efforts in the revision of the text. The authors adequately responded most questions, but I have still some comments and suggestions. The text would be ready for publication in ACP after the following is addressed.

**Response:** We thank the reviewer very much for the careful evaluation and valuable comments for our work. We revised the manuscript as much as possible respecting the reviewer's comments.

## Specific comments from Anonymous Referee #1 (comments are in italic)

** I believe that the abstract is still long. There are still the experimental information remaining.*

**Response:** We revised the abstract more concisely as can be seen in the revised abstract.

** About the type of particles (lines 271–295), I think that the authors are talking about "the type of hygroscopicity" during the cycle between humidification and dehumidification. Three particles were generated from the same stock solution, but the authors observed three different behaviors in the hygroscopicity. Using the wording of particle type may mislead us to think of three types of particles prepared by three different sources.*

**Response:** We agree with the reviewer that we are talking about "the type of hygroscopicity" of particles during the hygroscopic process, and as seen in the beginning of the section 3.1, we have explained that "Wet-deposited MBTCA aerosols exhibited three types of hygroscopic behaviors". In order not to cause any misleading, the sentence will be modified as below: "Wet-deposited MBTCA aerosols generated by the nebulization from a pure MBTCA solution exhibited three different types of hygroscopic behaviors, which are termed as "types 1, 2, and 3". (lines 225-226 in the marked revised version below).

The sentence at line 264 will be modified as "Specifically, the types of hygroscopicity of pure MBTCA particles were classified as".

** It seems that the authors overlooked my question on" the repeatability of the phenomenon of efflorescence during the humidification". Can you respond this question?*

**Response:** As explained at lines 317-321 in the marked revised version below, all the observed $Na_3M$ particles on the substrate (around 100 particles) behaved exactly in the same way with crystallization during humidification process and we think that this phenomenon is repeatable. And we've also explained at lines 283-285 in the marked revised version below that the efflorescence during humidification is not rare as it was also observed by other studies.

** I am not sure if the large size of the particles used in the levitation is the reason why the particle shrinkage could not be captured. The size change captured by a camera should be more apparent for large particles because the particle shrinkage is defined as the relative change in particle size. Let's say a few percent size decrease for the observation of the shrinkage relative to the particle size at low RH. The absolute size change should be larger for larger particles so that the size change can be more visible.*

**Response:** We agree with the reviewer. Actually, the optical image quality of the levitated particles was not as good as those in the see-through impactor system, which made the 2-D area plot less accurate and precise. However, the shrinkage of the particles before the deliquescence is not much important in our study and does not influence our observations regarding the hygroscopicity of the pure and mixture particles. We deleted the sentences at line 527-531 in the marked revised version below without deteriorating the context.

** Minor point:*

*Line 28: dissolve -> deliquesce*

**Response:** Modified as suggested (line 24 in the marked revised version).

# Hygroscopic behavior of aerosols generated from solutions of 3-methyl-1,2,3-butanetricarboxylic acid, its sodium salts, and its mixtures with NaCl

Li Wu[1], Clara Becote[2,3,4], Sophie Sobanska[2], Pierre-Marie Flaud[3,4], Emilie Perraudin[3,4], Eric Villenave[3,4], Young-Chul Song[1], Chul-Un Ro[1*]

[1]Department of Chemistry, Inha University, Incheon, South Korea

[2]Institut des Sciences Moléculaires, UMR CNRS 5255, University of Bordeaux, Talence, France

[3]University of Bordeaux, EPOC, UMR 5805, 33405 Talence cedex, France

[4]CNRS, EPOC, UMR 5805, 33405 Talence cedex, France

## Abstract

MBTCA (3-methyl-1,2,3-butanetricarboxylic acid), a low volatile, highly oxidized, secondary generation product of monoterpenes, is one of the most relevant tracer compounds for biogenic SOAs. In this study, laboratory-generated, micrometer-sized, pure MBTCA, mono-/di-/tri-sodium MBTCA salts, and MBTCA-NaCl mixture aerosol particles of four mixing ratios (molar ratios = 1:1, 1:2, 1:3, and 2:1) were examined systematically to observe their hygroscopic behavior by varying the relative humidity (RH) ~~from RH = ~95% to ~1% through a dehydration process, followed by a humidification process from RH = ~1% to ~95%~~, using in-situ Raman microspectrometry (RMS) assembled with either a see-through impactor where the particles were deposited on a Si wafer or a levitation system. ~~The hygroscopic behavior of pure MBTCA and MBTCA-NaCl mixture aerosol particles of three mixing ratios (molar ratios = 1:1, 1:2, and 1:3) were also examined using a levitation system mounted on in-situ RMS through a humidification process from RH = ~10% to ~80% after a quenching process from droplets, followed by dehydration from RH = ~80% to ~10%.~~ The pure MBTCA droplets effloresced at RH = ~30-57.8% and did not deliquesce until RH > 95%. The mono- and di-sodium MBTCA salt aerosols did not show clear efflorescence RH (ERH) and deliquescence RH (DRH). In contrast, the tri-sodium MBTCA salt exhibited ERH = ~44.4-46.8% and DRH = ~53.1%, during the hygroscopic experiment cycle. The mixture aerosols generated from solutions of MBTCA:NaCl = 1:1 and 2:1 showed no visible ERH and DRH in the see-

*Corresponding author. Tel.: +82 32 860 7676; Fax: +82 32 867 5604; E-mail: curo@inha.ac.kr

through impactor because of the partial and total consumption of NaCl, respectively, through chemical reactions during the dehydration process. The mixture particles with a 1:1 molar ratio in the levitation system exhibited a clear DRH at ~71% and ERH at ~50%. This suggests less reaction between the mixtures and a larger portion of NaCl remaining in the levitation system. The other mixtures of MBTCA:NaCl = 1:2 and 1:3 displayed single-stage efflorescence and deliquescence at ERH = ~45-50% and DRH = ~74%, respectively, because of the considerable amount of NaCl present in the mixture aerosols in both systems. Observations and Raman analyses indicated that only monosodium MBTCA salt aerosols could be formed through a reaction between MBTCA and NaCl. The reaction occurred more rapidly with a more elevated concentration of either MBTCA or NaCl, and the controlling factor for the reactivity of the mixtures depended mostly on the availability of $H^+$ dissociated from the MBTCA tricarboxylic acid. The lower degree of reaction of the mixture particles in the levitation system might be caused by the relatively airtight circumstance inside, i.e., the less release of HCl. ~~In addition, the quenching process, i.e., the starting point of the hygroscopicity experiments, induced the solidification of MBTCA, and further, a slow reaction between MBTCA and NaCl.~~ The study revealed that the interactions between the MBTCA and NaCl could modify the properties of the organic acid in the atmosphere, leading to enhanced capability of the probable heterogeneous chemistry in the aqueous aerosols.

## 1. Introduction

Chemical processes, such as gas-phase oxidations of airborne biogenic and anthropogenic volatile organic compounds (VOCs) by ozone ($O_3$), hydroxyl radical (OH), and nitrate radical ($NO_3$), and their condensed-phase reactions with preexisting aerosols, can promote the formation of increasingly oxidized and less volatile secondary organic aerosols (SOAs). SOAs are a ubiquitous and dominant fraction of the fine aerosol mass that exists as liquid, amorphous solid, semi-solid, and phase-separated aerosol particles (Jang et al., 2002; Hallquist et al., 2009; Jimenez et al., 2009; Virtanen et al., 2010; Koop et al., 2011; Bateman et al., 2015b; Shrivastava et al., 2015; Bernard et al., 2016; Pajunoja et al., 2016; Freedman, 2017; Shrivastava et al., 2017; Kim et al., 2018; Srivastava et al., 2018; Liu et al., 2019; Slade et al., 2019; Song et al., 2019; Wu et al., 2019a). These aerosols are of critical importance because of their ability to scatter and absorb solar radiation directly, to affect the number of CCN (cloud condensation nuclei)

through the formation of new particles and the growth of preexisting particles, and further impact the climate and human health (Haywood and Boucher, 2000; Topping et al., 2013; Poschl and Shiraiwa, 2015; Reid et al., 2018; Marsh et al., 2019). SOAs are highly dynamic, multiphase chemical systems with a range of volatility and solubility and model simulations have claimed that the phase state of SOAs differs according to the global locations and altitudes with an evolving relative humidity (RH), temperature, and particle composition (Kroll and Seinfeld, 2008; Shiraiwa et al., 2017).

Oxidative products of biogenic VOCs, such as monoterpenes (e.g., α- and β-pinenes), act as a dominant source of SOAs as they have high emission rates on a global scale and give considerable SOA yields, and they play a central role in new particle formation (Guenther et al., 1995; Lignell et al., 2013; Mutzel et al., 2016; Holopainen et al., 2017). Carboxylic acid-containing organic compounds comprise a large fraction of SOAs in the Northern Hemisphere (Yatavelli et al., 2015). An extremely low-volatile tricarboxylic acid, 3-methyl-1,2,3-butanetricarboxylic acid (MBTCA, $C_8H_{12}O_6$), has become one of the most relevant tracer compound for terpene SOAs (Jaoui et al., 2005; Szmigielski et al., 2007; Zhang et al., 2010; Donahue et al., 2012; Müller et al., 2012; Lai et al., 2015; Sato et al., 2016). In addition, it is also a few well-known compounds with a high O:C ratio that is formed in the oxidation of VOCs (Dunne et al., 2016). MBTCA is a second or later generation reaction product from monoterpenes by the OH-initiated oxidation of pinonic acid (PA) in the gaseous and aqueous phases and even at the air-water interface (Müller et al., 2012; Praplan et al., 2012; Aljawhary et al., 2016; Enami and Sakamoto, 2016). The MBTCA concentrations were found to be positively correlated with temperature because of the enhanced photochemical production of PA by OH radicals with increasing temperature (Hu et al., 2008; Zhang et al., 2010; Gómez-González et al., 2012; Miyazaki et al., 2012). A further reaction between MBTCA and OH radicals can result in $CO_2$ loss (Kostenidou et al., 2018). MBTCA was first observed at the Amazon basin and in summer aerosols from Ghent, Belgium (Kubátová et al., 2000; Kubátová et al., 2002). The compound was later found in the USA (Jaoui et al., 2005), Europe (Fu et al., 2009; Kourtchev et al., 2009; Zhang et al., 2010; Yasmeen et al., 2011; Gómez-González et al., 2012; Vogel et al., 2013; Kammer et al., 2018; Vlachou et al., 2019), Japan (Miyazaki et al., 2012), the polar regions (Hu et al., 2013), China (Hu et al., 2008; Ding et al., 2012; Li et al., 2013; Fu et al., 2014; Kang et al., 2018; Hong et al., 2019), and Australia (Cui et al., 2019). In addition, it has been observed in forest, marine,

mountainous, urban, and rural aerosols, with its levels ranging from 0.03 to 100 ng/m$^3$, and the level was generally higher in the fine particle fraction than in the coarse fraction (Zhang et al., 2010).

The ability of the aerosol particles to uptake water in the air is dependent on one of the most important physicochemical properties, i.e., the hygroscopicity (Jimenez et al., 2009; Chu et al., 2014; Tang et al., 2019; Wu and Ro, 2020). Hygroscopicity can help better understand the (i) aerodynamic properties, (ii) cloud-droplet nucleation efficiency, (iii) optical properties, and (iv) physicochemical changes through complicated heterogeneous chemical reactions of aerosol particles with various atmospheric gas-phase species. MBTCA was predicted to partition significantly into aerosol-liquid-water (ALW) (Aljawhary et al., 2016). Therefore, a study on the hygroscopic behavior of MBTCA is important for understanding its phase states better when it interacts with water vapor at different RHs as well as its impacts on the heterogeneous chemical reactions, atmospheric environment, and human health (Parsons et al., 2004; Mikhailov et al., 2009; Bateman et al., 2015a; Freedman, 2017; Slade et al., 2019). Atmospheric particles typically involve complex internal mixtures of organic and inorganic compounds (Shrivastava et al., 2017; Karadima et al., 2019). The interactions between organic and inorganic compounds may alter the chemical compositions of SOAs, which in turn affect their physicochemical properties, such as hygroscopicity (Rudich et al., 2007; Wu et al., 2011; Wang et al., 2015; Jing et al., 2016; Wang et al., 2018). Dicarboxylic acids (DCAs) can undergo reactions with inorganics, such as NaCl, resulting in Cl depletion and HCl liberation (Ma et al., 2013; Li et al., 2017). On the other hand, the interactions between tricarboxylic acids and inorganics have never been investigated.

In this study, in situ Raman microspectrometry (RMS) was used to examine the hygroscopic behavior, evolution of the chemical composition, phase states, and microstructures, and chemical reactivity of laboratory-generated, micrometer-sized aerosols generated from a pure MBTCA solution, mono-/di-/tri-sodium MBTCA salt solutions, and MBTCA-NaCl mixture solutions. RMS was assembled with either a see-through impactor, where the particles were deposited on a Si wafer, or a levitation system. The particles on the Si wafer were exposed to a hygroscopic measurement cycle, where they experienced a dehydration process first (by decreasing RH from ~95 to ~1%), followed by a humidification process (by increasing RH from ~1 to ~95%). The particles in the levitation system experienced a humidification process first (by increasing the RH from ~10 to ~80%) after quenching from droplets, followed by a

dehydration process (by decreasing RH from ~80 to ~10%). The deposited particles (~6.5 μm size in average in this study) may have some influences from the collecting substrate such as a facilitated heterogeneous nucleation, which can be eliminated in the levitation system due to the substrate-free and contactless properties. However, the particles in the levitation system are generally large in size (~80 μm in average in this study), which is less atmospherically relevant. And thus, the analysis of the particles in both systems is expected to give more detailed information on the hygroscopic behavior of MBTCA aerosols. NaCl, one of the major components of marine aerosols, was selected as the inorganic component since it was previously reported that organic acids contributed significantly to Cl depletion through a reaction with NaCl (Laskin et al., 2012). In situ Raman analysis could clearly identify MBTCA and its sodium salts during the hygroscopicity measurement despite NaCl being Raman inactive. To the best of the authors' knowledge, this is the first study on the hygroscopic behavior and chemical reactivity of MBTCA and its sodium salts thus far. The results are expected to promote more precise thermodynamic models (Clegg et al., 2003). The phase transitions were observed by monitoring the size changes together with the Raman spectra evolutions of the aerosol particles as a function of the RH. RMS can provide information on chemical functional groups, water contents, molecular interactions, and phase states of the aerosol particles. Such data can help understand the hygroscopic behavior of complex aerosol particles better (Lee et al., 2008; Li et al., 2017; Wang et al., 2017). The molecular characterization of organic aerosols can provide better insights into the potential mechanisms of SOA formation and transformation (or aging) (Hallquist et al., 2009). Scanning electron microscopy (SEM)/energy-dispersive X-ray spectroscopy (EDX) mapping was used to examine the elemental composition distribution in effloresced particles.

## 2. Experimental Section

### 2.1 Sample preparation

Pure 0.3 M solutions of NaCl (>99.9% purity, Sigma-Aldrich) and MBTCA (98%, Toronto Research Chemicals, TCR) were prepared. The mixture solutions of MBTCA and NaCl were prepared with molar mixing ratios of MBTCA:NaCl = 1:1, 1:2, 1:3, and 2:1. Mono-/di-/tri-sodium MBTCA salt solutions were obtained by mixing MBTCA and NaOH (>99.9% purity, Sigma-Aldrich) with molar ratios of

MBTCA:NaOH = 1:1, 1:2, and 1:3, respectively. A mixture solution of MBTCA and monosodium MBTCA salt with a molar mixing ratio of 1:1 was prepared as well. All the solutions were made by dissolving the chemicals in the ultrapure de-ionized (DI) water (18 MΩ, Millipore Direct-QTM). Aerosol particles were generated by nebulizing the solutions using a single jet atomizer (HCT4810) on the Si wafer substrates (MTI Corporation, 99.999% purity). The size of the droplets examined at RH > 90% ranged from 1 to 15 μm.

**2.2 In situ Raman microspectrometry (RMS) for particles deposited on a Si wafer**

During the hygroscopic measurements, in situ RMS was performed under a controlled RH to observe the hygroscopic behavior, structural changes, and chemical compositional variations of the aerosols generated from the solutions. The apparatus consisted of three parts: (A) see-through impactor, (B) Raman microscope/spectrometer, and (C) humidity-controlling system. The Si wafer substrate was mounted on the impaction plate in the see-through impactor. A more detailed discussion of the impactor and humidity-controlling system can be found elsewhere (Gupta et al., 2015). Briefly, the RH inside the impactor was controlled by mixing dry and wet (saturated with water vapor) $N_2$ (99.999% purity) gases. The flow rates of total 4 $L \cdot min^{-1}$ of the dry and wet $N_2$ gases were controlled by two mass flow controllers to obtain the desired RH in the range of ~1−95%, which was monitored using a digital hygrometer (Testo 645). The digital hygrometer was calibrated using a dew-point hygrometer (M2 Plus-RH, GE) to provide RH readings with ±0.5% reproducibility. The Raman spectra and optical images of the aerosol particles were recorded by Labspec6 using a confocal Raman microspectrometer (XploRA, Horiba Jobin Yvon) equipped with a ×50, 0.5 numerical aperture objective (Olympus). An excitation laser with a wavelength of 532 nm and 6 mW power was used, and the scattered Raman signals were detected at specific RHs during the hygroscopic measurements using an air-cooled multichannel charge-coupled device (CCD) detector. The data acquisition time for each measurement was 120 s. The spectral resolution was 1.8 $cm^{-1}$ using 1800 gr/mm. The optical images were recorded continuously in RH = 1% steps with a size of 904×690 pixels during the first dehydration (by decreasing RH from ~95 to ~1%), followed by the humidification (by increasing RH from ~1 to ~95%) experiments using a top video camera assembled in the Raman instrument and processed using an image analysis software (Matrox, Inspector v9.0). Each

humidity condition was sustained for at least 2 mins in order to provide an enough time for condensing or evaporating of water. The changes in particle size with the RH were monitored by measuring the particle 2-D area in the optical images to generate hygroscopic curves. These curves are represented by the area ratio ($A/A_0$) as a function of RH, where the 2-D projected aerosol area at a given RH ($A$) is divided by that at the end of the dehydration process ($A_0$) (Ahn et al., 2010). All hygroscopic experiments were conducted at room temperature (T = 22±1℃). Aerosol particles generated from a pure NaCl aqueous solution to check the accuracy of the system showed typical hysteresis curves with deliquescence RH (DRH) = 75.5(±0.5)% and efflorescence RH (ERH) = 46.3–47.6% as shown in Fig. S2, which are consistent with the theoretical and reported values.

### 2.3 SEM/EDX X-ray mapping of effloresced particles deposited on Si wafer

SEM/EDX X-ray mapping was performed for effloresced particles to determine the morphology and spatial distribution of the chemical elements after the hygroscopicity measurements of individual particles (Ahn et al., 2010; Gupta et al., 2015). The measurements were carried out using a Jeol JSM-6390 SEM equipped with an Oxford Link SATW ultrathin window EDX detector. The resolution of the detector was 133 eV for Mn Kα X-rays. The X-ray spectra and elemental X-ray maps were recorded under the control of Oxford INCA Energy software. A 10 kV accelerating voltage and 0.7 nA beam current were used, and the typical measuring time for the elemental mapping was five minutes. An elemental quantification procedure, which is well described elsewhere (Wu et al., 2019a), was used for obtaining the elemental concentration.

### 2.4 In situ RMS assembled with a levitation system

The levitation experimental set up consisted of coupling an acoustic (ultrasonic) levitator equipped with an environmental cell to an RMS, as shown in Fig. S1. The theory of acoustic levitation is described in detail elsewhere (Seaver et al., 1989). An ultrasonic levitator was modified (APOS BA 10, Tec5, Germany) to be installed within an environmental levitation cell consisting of two quartz windows, allowing the particle analysis (Seng et al., 2018). Two inlet/outlet valves were used for gas supplies to modify the relative humidity (RH) inside the cell. A sensor (SHT75 Sensirion) was placed in the cell to

control the RH and temperature. The RH inside the chamber was controlled by mixing dry and wet Ar gases with a flow rate of 200 $mL \cdot min^{-1}$ in the range of 10-80%(±1%) RH, and the temperature was T = 25±3 °C, making the experiments close to static flow conditions. The control of humidity and temperature allows limited droplet evaporation and long-term monitoring of the particles. The RMS measurements were performed with a LabRAM HR Evolution confocal spectrometer (Horiba Scientific, S.A) at certain RHs first during humidification and then during dehydration. The instrument was equipped with an ×50, 0.45 numerical aperture Olympus objective (WD = 13.8 mm) and a He-Ne laser (λ = 632.8 nm – 6 mW) with a theoretical lateral resolution of ~2 μm, and a depth of the laser focus corresponding to 16 μm with a Δz limit ≥ ±3 μm. The cell was mounted on an XYZ stage under the objective, allowing an adjustment of the droplet in the optimal position for the measurements. The mean size of the initial droplet injected in the levitator was 80 μm. The Raman spectra and optical images recorded at specific RHs were analyzed similarly to those obtained on the Si wafer.

### 2.5 Measurement of acid dissociation constants of MBTCA

MBTCA is a tri-carboxylic acid with three acid dissociation constants. To determine the three constants, a 0.02 M, 5 ml MBTCA solution was titrated with a 0.1 M NaOH solution, where the constants were determined based on the Henderson-Hasselbalch equations (Harris, 2012):

$$H_3M + OH^- \rightarrow H_2M^- + H_2O \quad pH = pKa_1 + \log([H_2M^-]/[H_3M])$$

$$H_2M^- + OH^- \rightarrow HM^{2-} + H_2O \quad pH = pKa_2 + \log([HM^{2-}]/[H_2M^-])$$

$$HM^{2-} + OH^- \rightarrow M^{3-} + H_2O \quad pH = pKa_3 + \log([M^{3-}]/[HM^{2-}])$$

where $H_3M$, $H_2M^-$, $HM^{2-}$, and $M^{3-}$ represent aqueous MBTCA, mono-, di-, and tri-sodium MBTCA anions, respectively. The $pKa_1$, $pKa_2$, and $pKa_3$ are the pHs when $[H_3M]$, $[H_2M^-]$, and $[HM^{2-}]$ equal $[H_2M^-]$, $[HM^{2-}]$, and $[M^{3-}]$, respectively, during the acid-base titration. Specifically, when NaOH was added at 0.5, 1.5, and 2.5 ml, the corresponding pHs of the solution are the three constants, which were 3.59, 4.85, and 6.79. Fig. 1 shows the calculated titration curve of MBTCA using the three determined Ka values, which is the same as the experimentally obtained titration data, supporting the validity of the Ka values, which were not reported so far.

## 3. Results and Discussion

### 3.1 Hygroscopic behavior of pure MBTCA particles

Wet-deposited MBTCA aerosols generated by the nebulization from a pure MBTCA solution exhibited three different types of hygroscopic behaviors, which are termed as "types 1, 2, and 3". As shown in Fig. 2, during the dehydration process, the exemplar droplets of types 1 and 2 shrank continuously with decreasing RH due to water evaporation until RHs = 58.4% and 40%, and then effloresced promptly at RH = 57.8% and gradually at RH = 39 - 35%, respectively. The effloresced particles maintained their size and shape with further decreases in RH. Whereas, the type 3 aerosols decreased continuously in size without a distinct change from RH = 94% to RH = 3% during the dehydration process. During the humidification process, types 1 and 2 particles kept the same size and shape until RH = ~90%, while type 3 particles experienced a gradual shrinkage at RH = 34-36.7% and remained the same until RH = ~85%. Fig. 2 also presents the corresponding optical images and in situ Raman spectra to assess the structural evolution of the MBTCA aerosols during the dehydration and humidification processes. Briefly, Raman peaks at ~1411 - 1420 $cm^{-1}$, ~1460 and ~2950 $cm^{-1}$, ~1660 - 1730 $cm^{-1}$, and ~3420 - 3475 $cm^{-1}$ are for vibrations of C=O from $COO^-$, CH, C=O from COOH, and OH from water, respectively (Edsall, 1937; An et al., 2016). The redshift of the C=O peak (from COOH) from 1715 to 1660 $cm^{-1}$ with decreasing FWHH (full width at half height), which is consistent with the standard MBTCA crystal, and the irregular shape and rough surface of types 1 and 2 aerosols at RH = 57.8% and 35%, respectively, confirmed that the particles effloresced into a solid phase. The optical images in the inset above the hygroscopic curve of the type 2 particles showed gradual efflorescence at RH = 39 – 35%. The water peak at ~3475 $cm^{-1}$ disappeared as well after the efflorescence. In contrast, type 3 aerosols maintained a circular morphology until RH = 3%, as shown in the optical images in Fig. 2, even though an overlapped C=O (from COOH) peak at 1660 - 1680 $cm^{-1}$ appeared during the dehydration process, and the water peak became undetectable, as shown in the Raman spectra at RHs = 45% and 3%, suggesting an amorphous/solid-state and the presence of an activation barrier or diffusional resistance to homogeneous nucleation required for the crystallization of MBTCA droplets as efflorescence is a kinetically controlled process (Martin, 2000; Freedman, 2017). Previous studies reported that α-pinene SOAs were very likely to exist as a highly viscous semisolid or even glassy state at low humidity (Saukko et al., 2012; Renbaum-Wolff et al., 2013; Berkemeier et al., 2014; Dette et al., 2014; Kidd et al., 2014;

Song et al., 2016; Lessmeier et al., 2018). In addition, many organic substances, such as carboxylic acids, carbohydrates, and proteins, tend to form amorphous rather than crystalline phases upon the drying of aqueous solution droplets (Mikhailov et al., 2009). During the humidification process, the Raman spectra and morphology remained unchanged for types 1 and 2 particles until RH = ~90%, where a slight decrease in morphology was observed due to structural re-arrangements by the absorption of moisture on the lattice imperfections (Gysel et al., 2002). Besides, the substrate can also affect this shrinkage. Especially, the hydrophilic substrate (such as Si wafer used in this study) seems to favor the phenomenon (Eom et al., 2014). Type 3 particles during the humidification process became irregular in shape, and the overlapped C=O (from COOH) peak shifted to 1660 $cm^{-1}$ at RH = 36.7%, as shown in the optical image and Raman spectrum, indicating the formation of solids. With the further increase in RH, particles maintained their size and shape until RH = 85%, where they started to decrease in size due to a re-arrangement in structure. All types of MBTCA particles maintained the crystal phase until RH = 95%.

Specifically, the types of hygroscopicity of pure MBTCA particles were classified as, "type 1: with a prompt efflorescence at ~50% RH during dehydration; type 2: with a gradual efflorescence at ~35% RH during dehydration; type 3: with a gradual efflorescence at ~37% RH during humidification", based on their different behavior when efflorescence occurred. The different efflorescence behavior was attributed to different nucleation mechanisms: heterogeneous nucleation for types 1 and 2 particles (seed-containing), and homogeneous nucleation for type 3 particles (pure). MBTCA powders, which was used for making the MBTCA solution, has intrinsic unknown impurity of 2%, and they were used without any purification. When MBTCA powders were dissolved in DI water and particles were generated by the nebulization of the aqueous solution using $N_2$ gas, impurities were either absent or associated with the droplets. The impurities existed in types 1 and 2 particles after nebulization, acting as seed crystals to induce efflorescence. Aqueous moieties in particles were reported to effloresce more easily by heterogeneous nucleation in the presence of seeds (Schlenker and Martin, 2005; Li et al., 2014; Gupta et al., 2015). The lower ERH and gradual efflorescence of type 2 compared to type 1 particles might be due to the less amount of impurities. Type 3 particles contain negligible or no seed crystals, and large kinetic barrier and/or diffusional resistance make the formation of the crystal structure difficult owing to the decreasing availability of condensed water during dehydration, so that they did not experience any

efflorescence. A similar situation was observed for $NH_4NO_3$, $NaNO_3$, and $NH_4HSO_4$ particles (Lightstone et al., 2000; Hoffman et al., 2004; Gibson et al., 2006; Kim et al., 2012; Jing et al., 2018; Sun et al., 2018; Wu et al., 2019b). The Si substrates used in this study could also facilitate efflorescence (Eom et al., 2014; Wang et al., 2017). The efflorescence during humidification like type 3 particles was previously reported for Amazonian rain forest aerosols (Pöhlker et al., 2014) and the laboratory-generated NaCl–$MgCl_2$ mixture particles (Gupta et al., 2015). Thus, this phenomenon is not rare. And it was claimed that the aerosol particles initially had amorphous or poly-crystalline structures and underwent restructuring through kinetic water and ion mobilization in the presence of sufficient condensed water, resulting in overcoming the kinetic barrier and crystallization during humidification.

Among 100 particles, type 1-3 particles accounted for approximately 25%, 5%, and 70%, respectively, suggesting that MBTCA has slow homogeneous nucleation rate. Based on the experimental results, MBTCA droplets have DRH > 95% and ERH = 30–58%. This is the first study reporting the hygroscopic properties of MBTCA. A previous study showed that MBTCA was not hydrated significantly in the ambient atmosphere (Kildgaard et al., 2018), and our results also implied that the MBTCA solids stay in the air once they effloresced, based on our results.

### 3.2 Hygroscopic behavior of mono-/di-/tri-sodium MBTCA salt aerosols

The hygroscopicity and Raman spectra of mono-/di-/tri-sodium MBTCA salt aerosols (hereafter, denoted as $NaH_2M$, $Na_2HM$, and $Na_3M$, respectively) were studied to examine the hygroscopic behavior and estimate the chemical reactivity of MBTCA with NaCl. Figs. 3(a)-(c) show the 2-D projected area ratio plot of aerosol particles generated from 0.3 M $NaH_2M$, $Na_2HM$, and $Na_3M$ aqueous solutions as a function of the RH together with the corresponding optical images and Raman spectra recorded at specific RHs. As shown in Figs. 3(a) and (b), $NaH_2M$ and $Na_2HM$ aerosols shrank and grew continuously without a phase transition during the dehydration and humidification processes, respectively, which is also reflected in the optical images and Raman spectra, where they maintained their circular morphology only with a change in size and the same Raman peak patterns and positions with small variations in the relative peak intensities during the entire process. The water peak at ~3400-3500 $cm^{-1}$ can still be observed at the end of the dehydration process. Even after being kept in a desiccator for two months, $NaH_2M$ and $Na_2HM$

particles still showed the same shapes and Raman spectra with those at RHs = 3.4% and 2.8%, respectively. These results indicate the non-crystallizable properties and supersaturated amorphous phase state of the particles. The $Na_3M$ particles behaved differently as they did not crystallize during the dehydration process. On the other hand, the aerosols exhibited efflorescence at RH = 46.8% during the humidification process (Fig. 3(c)), deliquesced to become a droplet at RH = 53.1%, and grew continuously after that with increasing RH. The Raman spectra of the $Na_3M$ particles in Fig. 3(c) showed that the peak at 1420-1460 $cm^{-1}$ became two sharp peaks when the particles effloresced, and the OH peak at 3400 $cm^{-1}$ indicates that $Na_3M$ particles possibly exist in the hydrated form. The $Na_3M$ particles behaved analogously to type 3 MBTCA particles, which might be due to their similar structures when all three COOH in MBTCA were replaced with COONa upon the reaction between MBTCA with NaOH. Since all the observed $Na_3M$ particles on the substrate (around 100 particles) behaved exactly in the same way with crystallization during humidification process, the major contribution to the crystallization of $Na_3M$ particles is homogeneous crystallization, instead of heterogeneous crystallization induced by impurities and Si substrate effect. Based on the top Raman spectra of aqueous MBTCA, $NaH_2M$, $Na_2HM$, and $Na_3M$ aerosols in Figs. 2 and 3, the ratios of the CH peak at ~1460 $cm^{-1}$ to the C=O peak at ~1720 $cm^{-1}$ (from COOH) and to the C=O peak at ~1420 $cm^{-1}$ (from $COO^-$) increased and decreased in the order of MBTCA, $NaH_2M$, $Na_2HM$, and $Na_3M$ because of their reduced and elevated levels of COOH and $COO^-$, respectively.

### 3.3 Hygroscopic behavior of MBTCA-NaCl mixture aerosols

Aerosols were generated by the nebulization of MBTCA-NaCl mixture solutions of molar mixing ratios of MBTCA:NaCl = 1:1, 1:2, 1:3, and 2:1 and deposited on Si wafer substrates, while maintaining the entire hygroscopic measurement system at RH > 90%. The hygroscopic behavior was investigated for ~10 individual aerosols of each mixing ratio, which are discussed in the following sections.

#### 3.3.1 Aerosols generated from solutions of MBTCA:NaCl = 1:1 and 2:1

Fig. 4 presents the hygroscopic curves of representative aerosols nebulized from solutions of MBTCA:NaCl mixtures at different molar ratios (1:1 and 2:1) along with the corresponding optical

images and Raman spectra at specific RHs. During the dehydration process, the circular liquid droplets decreased in size gradually without any noticeable phase change. The Raman peak patterns were maintained only with the C=O peak at 1721 $cm^{-1}$ (from COOH) shifting mildly rightwards, the water peak at 3466 $cm^{-1}$ becoming undetectable, and the relative peak intensities at ~1411, 1457, and 1721 $cm^{-1}$ varied when the RH was as low as 1.2%, indicating that the liquid droplets formed amorphous solids. The peak at 1680 $cm^{-1}$ on the Raman spectra of MBTCA:NaCl = 2:1 at RH = 1.2% suggested that the amorphous structure of the remaining MBTCA had been retained. Both MBTCA and NaCl have their DRHs and ERHs. Therefore, a step-wise efflorescence would happen if it is assumed that the mixture aerosols are an MBTCA-NaCl binary system, i.e., a component of the aqueous droplets precipitates first at their specific ERHs depending on their mixing ratios, and the second crystallization from the remnant eutonic solution occurs at their mutual ERH (MERH) with further decreases in RH, which is independent of the mixing ratios, generally forming a heterogeneous, core-shell crystal structure owing to the two-stage crystallization process (Ge et al., 1996; Gupta et al., 2015). However, the particles of MBTCA:NaCl = 1:1 and 2:1 mixing ratios did not follow the step-wise transitions in the present study, revealing that the aerosols do not belong to the MBTCA-NaCl binary system and the chemical compositions evolved during the hygroscopic experiment due to the reaction between MBTCA and NaCl, which will be discussed later.

During the humidification process, aerosol particles of two mixing ratios grew continuously when the RH was increased from 1.2% to 90% with C=O peak (from COOH) shifting back to ~1721 $cm^{-1}$ and the water peak becoming significant, as shown in Fig. 4. Several small crystal-like spots, which are marked by a dotted circle on the inset optical image beside the hygroscopic curve in Fig. 4(a), appeared in the particles with the mixing ratio of MBTCA:NaCl = 1:1 when the RH was increased to 67.2% and dissolved completely at RH = 71.2%. As the Raman spectra did not show any signals of the crystallized organics and RH = 71.2% is close to the DRH of pure NaCl (75(±0.5)%), the crystal-like moieties should result from the effloresced NaCl. The more noticeable water peak in the Raman spectrum taken at RH = 71.2% than that at RH = 67.2% also supports that the NaCl dissolved at RH = 71.2% as NaCl is quite hygroscopic (Li et al., 2017). No phase transition of NaCl was detected during the dehydration process, probably because the supersaturated organic moiety inhibited the crystallization of NaCl. The observation of effloresced particles during the humidification process might be caused by the structural re-arrangement

of the amorphous particles upon the slow and continuous absorption of moisture with increasing RH (Mikhailov et al., 2009), leading to less restriction to NaCl crystallization. Indeed, organics in organic-inorganic mixture aerosols were reported to be a minor disturbance to the DRH of inorganic salts; in contrast, they may markedly decrease the ERH of inorganic salts depending on the organic type (Parsons et al., 2004).

### 3.3.2 Aerosols generated from solutions of MBTCA:NaCl = 1:2 and 1:3

Fig. 5 shows the hygroscopic curves of aerosol particles nebulized from solutions of MBTCA:NaCl with molar mixing ratios of 1:2 and 1:3, together with the corresponding optical images and Raman spectra at the transition RHs. During the dehydration process, droplets from the solutions of MBTCA:NaCl = 1:2 and 1:3 decreased gradually in size owing to water evaporation until a single-stage transition was observed at RHs = 47.2-46.5% and 46.7-45.8%, respectively, where the particle shape became less circular in the optical images. At this point, the following were observed in the Raman spectra: the water peak at 3455 $cm^{-1}$ disappeared; the C=O peak at ~1722/1720 $cm^{-1}$ (from COOH) shifted slightly rightwards; the relative peak intensities at 1417/1416, 1461, and 1722/1720 $cm^{-1}$ varied. With the further decreases in RH until ~6%, the particles kept their size and shape. During the humidification process, all particles of MBTCA:NaCl = 1:2 and 1:3 maintained their structure until RHs = 50% and 40%, respectively, where they experienced a size decrease due to structural re-arrangement until RH = ~70%, grew continuously to become circular at RH = ~73%, and totally deliquesced into homogeneous droplets at RHs = 73.9% and 74.5%, respectively. Particle size and water peak increased rapidly, and the C=O peak (COOH) shifted back to 1720 $cm^{-1}$. Upon a further increase in RH, they grew continuously by water absorption. The ERH and DRH were attributed to the NaCl moiety as the Raman spectra maintained the peak patterns during the entire process, and the organic components condensed onto the NaCl crystal core almost simultaneously as an amorphous shell when efflorescence occurred, which is also indicated by the optical images. Before the complete deliquescence of the NaCl crystal core, the water peak at ~3455 $cm^{-1}$ in the Raman spectra and the optical images at RH = 72.4% and 73.8% of the particles from the MBTCA:NaCl = 1:2 and 1:3 solutions show that the organic shell was in the liquid phase, meaning that the mixture particles were in a solid-liquid equilibrium state (Sun et al., 2018). The Raman spectra shown

in the figures were all obtained in the center of the particles. The Raman spectra were obtained both at the center and the edge of the particles for comparison during the measurement when the heterogeneity appeared during the hygroscopic measurements. The spectra from the center and the edge were different only in the intensity since NaCl is Raman inactive. As shown in the Fig. S3, the Raman spectra which were obtained from the center and the edge of an exemplar MBTCA:NaCl = 1:3 particle during the humidification process, match well after normalization to the CH peak at 1460 $cm^{-1}$.

All the particles from MBTCA:NaCl = 1:2 and 1:3 solutions showed hysteresis curves with ERHs in the range of 46.7-45.2% and 47.2-45.6%, respectively, and DRHs = 73.9(±0.3)% and 74.5(±0.3)%, respectively.

### 3.3.3 Chemical reactivity of aerosols generated from MBTCA−NaCl mixture solutions

The first Raman spectra of the aerosols generated from MBTCA-NaCl mixture solutions in Figs. 4 and 5 were obtained before the dehydration process, which are comparable to that of pure MBTCA droplet particle in Fig. 2 except for a much stronger free water peak at 3450-3470 $cm^{-1}$ due to the presence of a more hygroscopic NaCl moiety. This suggests that upon nebulization from the solutions, the mixture droplets were mostly the MBTCA-NaCl binary system. The Raman spectra obtained at the beginning of the dehydration process and the end of the humidification process revealed increased and decreased ratios of the CH peak at ~1460 $cm^{-1}$ to the C=O peaks at ~1720 $cm^{-1}$ (from COOH) and ~1412 $cm^{-1}$ (from $COO^-$), respectively, which implies that the reaction between MBTCA and NaCl occurred during the hygroscopic experiment, leading to the decreased and increased levels of the COOH and $COO^-$ moieties, respectively. It is worth noticing that the dehydration and humidification curves of the MBTCA-NaCl mixtures did not overlap with each other mainly because of the different amounts of NaCl in the dehydration and humidification processes. As shown in the Fig. S2, NaCl is quite hygroscopic with around four times change in 2-D area after deliquescence, so the decreased amount of NaCl in the mixtures also lead to the smaller 2-D area when the MBTCA-NaCl mixture particles experienced hygroscopic growth during the humidification process, compared to those before dehydration. Fig. 6(a) presents the Raman spectra of particles generated from MBTCA:NaCl = 1:1, 1:2, and 1:3 solutions together with that of $NaH_2M$ particles obtained at the end of humidification by normalizing to the CH peak at 1458 $cm^{-1}$.

The C=O peak intensities at 1720 $cm^{-1}$ (from COOH) and 1412 $cm^{-1}$ (from $COO^-$) of the particles generated from the mixture solutions were higher and lower, respectively, than those of the $NaH_2M$ particle, suggesting that the aerosols generated from the MBTCA-NaCl solutions produced only $NaH_2M$ as the reaction product between MBTCA and NaCl, regardless of the mixing ratios. The droplet particles after the humidification process were present as an MBTCA-NaCl-$NaH_2M$ ternary system with varying compositions. As the first acid dissociation constant of MBTCA ($pKa_1 = 3.59$) is more than 1 and 3 orders of magnitude larger than the second ($pKa_2 = 4.85$) and third ($pKa_3 = 6.79$), respectively, $H_2M^-$ is more abundant than $HM^{2-}$ and $M^{3-}$. The chemical reaction between NaCl and MBTCA would occur in the aqueous phase as follows:

$$MBTCA(aq) + H_2M^-(aq) + H^+(aq) + Na^+(aq) + Cl^-(aq) \rightarrow MBTCA(aq) + H_2M^-(aq) + Na^+(aq) + Cl^-(aq) + HCl(g)\uparrow \rightarrow NaH_2M\ (+ MBTCA, amorphous) + NaCl(s)\ after\ the\ efflorescence$$

The $NaH_2M$ particles may exist as amorphous particles, as described before in section 3.2. Raman spectra of standard aerosols generated from solutions of MBTCA:$NaH_2M$ = 0:1, 1:1, and 1:0 were obtained at different RHs to estimate the chemical reactivity of the aerosol particles generated from the MBTCA-NaCl mixture solutions, which were used as a calibration curve to help determine the relative MBTCA and $NaH_2M$ contents in the aerosols at specific RHs. The estimation of the chemical reactivity between malonic acid and NaCl performed in the similar way was reported in a previous study (Li et al., 2017). The Raman spectra of MBTCA, $NaH_2M$, and mixture aerosols of MBTCA:$NaH_2M$ = 1:1 obtained at RH = 90% and normalized to the $CH_3$ peak at 1460 $cm^{-1}$ showed that the intensity ratio of the two peaks at 1460 $cm^{-1}$ ($CH_3$) and ~1720 $cm^{-1}$ (C=O from COOH) (i.e., $I_{1460}/I_{1720}$) increased with increasing $NaH_2M$ level because of the decreased COOH content, as shown in Fig. 6(b). The ratio, $I_{1460}/I_{1720}$, for each standard aerosol exhibited good linearity as a function of RH, as shown in Fig. 7(a), where the mean values obtained from 10 aerosols of each standard aerosol sample are plotted with error-bars. The Raman intensity ratios of the standard aerosols increased with decreasing RH because the C=O stretching vibrations of the free COOH group in the aqueous phase and the intramolecular hydrogen-bonded COOH

group in the supersaturated phase become weaker and stronger (Bertran et al., 2010), respectively, with decreasing RH during the dehydration process.

The dependency of the $I_{1460}/I_{1720}$ ratios on RH can be used to estimate the MBTCA and $NaH_2M$ (monosodium MBTCA salt) contents in the NaCl-MBTCA aerosols at specific RHs based on the calibration curve and to calculate the further reactivity. The chemical reactivity of the mixtures is represented as the degree of the reaction, which is defined as the ratio of consumed to the original amount of the limiting reactant. For example, for aerosols from solutions of MBTCA:NaCl = 2:1 and 1:2, NaCl and MBTCA are the limiting reactants, respectively. Fig. 7(b) shows the degree of the reaction of aerosols generated from solutions of each mixing ratio, where the mean degree of reaction has ~1.5-4% deviations owing to statistical variations in the Raman peak intensities caused by the baseline correction procedure and the uncertainties involved in the calibration measurements. The reactivity was estimated at five stages during one cycle hygroscopic experiment.

*Stage 1;* At the beginning of the hygroscopic experiment, no reaction occurred for all the mixed droplets based on their Raman spectra, i.e., the degree of the reaction is 0.

*Stage 2;* As the RH decreased during the dehydration process, the reaction continued in the aqueous aerosols until efflorescence of the droplets with mixing ratios of MBTCA:NaCl = 1:2 and 1:3 had occurred, and until the water content of the aerosols with mixing ratios of MBTCA:NaCl = 1:1 and 2:1 became insignificant. The degrees of the reaction of aerosols with mixing ratios of 1:1, 1:2, and 1:3 were approximately 30%, whereas that of 2:1 approached 85%.

*Stage 3;* The reaction of aerosols generated from the solution of mixing ratio of MBTCA:NaCl = 2:1 was complete at the end of the dehydration process, indicating the total consumption of NaCl and the formation of an MBTCA:$NaH_2M$ = 1:1 mixture aerosol. The Raman spectra of the aerosols with mixing ratios of MBTCA:NaCl = 1:1, 1:2, and 1:3 at the end of the dehydration process were unsuitable for the reactivity estimation mostly due to their heterogeneous structure in the presence of a NaCl core.

*Stages 4 and 5;* The reaction proceeded after deliquescence when the free $H^+$ and $Cl^-$ became available again for aerosols with mixing ratios of MBTCA:NaCl = 1:1, 1:2, and 1:3, and a small increase in the degree of reaction (~5%) was observed at the end of humidification for these mixture droplets.

Most of the reactions occurred in the aqueous phase during the dehydration process with considerable amounts of aqueous $H^+$ from MBTCA and $Cl^-$ from NaCl available for HCl liberation. During the entire experiment, the reactivity followed the sequence of MBTCA:NaCl = 2:1 > 1:3 > 1:2 > 1:1, where the reactivity appeared to be enhanced when either of the reactants is enriched. On the other hand, the reaction was complete only when aqueous $H^+$ was sufficiently available, i.e., the reaction depended mostly on the triacid level. The real-time aerosol mixture components based on the reactivity estimation of each mixing ratio at specific RHs are shown on the hygroscopic curves in Figs. 4 and 5.

The morphology and elemental distribution of effloresced MBTCA-NaCl particles were examined by SEM/EDX. Figure 8(a) shows the secondary electron images (SEIs) of the exemplar particles of each mixing ratio. The elemental X-ray maps for MBTCA:NaCl = 1:1 and 1:2 particles suggest that the NaCl solid moiety (represented by Na and Cl X-ray maps) crystallized homogeneously at small spots inside the organic moiety. For MBTCA:NaCl = 1:3 particles with a significant amount of NaCl, the NaCl solid existed as a core surrounded by the organic moiety. The organic mixture of MBTCA and $NaH_2M$ (represented by C and Na) condensed onto the NaCl core almost simultaneously when efflorescence occurred, while maintaining a relatively circular morphology, even after being inserted into the vacuum SEM chamber, which also indicates the low crystallization tendency of the organic moiety. The different shapes of organic shell-inorganic core structures depending on the organic mass fraction and RH are reported elsewhere (Karadima et al., 2019). The homogeneous structure of C and Na and the absence of Cl for particles with mixing ratios of MBTCA:NaCl = 2:1, as shown in the corresponding SEIs and X-ray spectrum in Figs. 8(a) and (b), confirmed that the reaction was complete at the end of the dehydration process. The reaction between MBTCA and NaCl and the changes in the microstructures after the reaction are expected to have some atmospheric implications since they may have enhanced ability to facilitate

561 further heterogeneous reactions in the atmosphere because of their low crystallization property. Na (from
562 both $NaH_2M$ and NaCl) and Cl (from NaCl) levels were used to estimate the degrees of reaction for the
563 MBTCA:NaCl = 1:1, 1:2, 1:3, and 2:1 systems, which were estimated to be ~25%, ~30%, ~37%, and
564 100%, respectively, with well matching to those from the Raman analysis by 5-8% differences.
565
566 **3.4 Hygroscopic behavior of pure MBTCA and MBTCA−NaCl mixture particles in the levitation**
567 **system**
568 The data acquired from the levitation system for contactless experiments on particles of ~80 μm were
569 used to compare with those obtained for aerosols on the Si wafer in the see-through impactor. The droplets
570 were introduced into the levitator and dried rapidly at RH = ~10% within 15 minutes (first rapid
571 dehydration, i.e., a quenching process), and humidified progressively to RH = 80%. Once RH = 80%, the
572 particles were dehydrated gradually until RH = ~10% (second dehydration).
573 Two types of hygroscopic behavior of pure MBTCA particles were observed, corresponding closely
574 to types 1 and 3 aerosol particles in the see-through impactor system, due to heterogeneous crystallization
575 induced by impurity seed crystals and homogeneous crystallization, respectively, confirming that once
576 the MBTCA particles overcome the kinetic barrier and effloresce into solids, they no longer capture water
577 significantly. The ERH was ~49-54%. The Raman spectra and optical images are not shown separately.
578 The Raman spectra and optical images of particles composed of MBTCA:NaCl = 1:1, 1:2, and 1:3
579 mixing ratios are shown in Fig. 9. After the first rapid dehydration of the particles, the existence of peaks
580 at 1655 and 1720 $cm^{-1}$ was observed for all the mixtures, and the relative intensity of the peak at ~1720
581 $cm^{-1}$ increased with the increase of the NaCl content, suggesting the formation of the mixture of solid
582 MBTCA and amorphous moiety either from MBTCA or $NaH_2M$. During the humidification process, the
583 Raman peak at 1720 $cm^{-1}$ and the particle size grew continuously with increasing RH. Transitions were
584 observed at RH = ~71%, ~74.5%, and ~75% for MBTCA:NaCl = 1:1, 1:2, and 1:3 mixture particles,
585 respectively, with the water peak at ~3500 $cm^{-1}$ becoming significant for the three compositions~~. However,~~
586 ~~the shrinkage of the particles before deliquescence was not captured for the levitated particles, as the~~
587 ~~particles are too big (~80 μm in average) for the structural rearrangement to be observed, and the 2-D~~
588 ~~optical images of the particles were used for plotting the hygroscopic curves even though the particles~~

~~were levitated, which might lead to some missing information on the 3-D level.~~The observed transition points were attributed to the deliquescence of NaCl within the particle with the MBTCA moiety partially remaining as a solid phase, and the elevated NaCl content strongly enhanced the ability of the particles to uptake water. The peak related to the solid portion at 1655 $cm^{-1}$ disappeared only for the MBTCA:NaCl = 1:3 mixture particles at the end of humidification, suggesting that the particle had transformed completely into a droplet. During the second dehydration process, the particles showed the entire release of water, as illustrated by the disappearance of the peak at 3500 $cm^{-1}$ at RH = ~50%, i.e., the ERH, for all the mixtures while maintaining the peak patterns and positions until the lowest RH. The Raman spectra recorded at the end of dehydration revealed both solid and amorphous phases for the MBTCA:NaCl = 1:1 and 1:2 mixtures due to the existence of the peaks at 1655 and 1720 $cm^{-1}$. In contrast, only the 1720 $cm^{-1}$ associated with the amorphous composition was observed for the MBTCA:NaCl = 1:3 mixture, suggesting that the reaction between MBTCA and NaCl was facilitated extensively by the increased NaCl concentration while absorbing sufficient moisture. The conspicuous DRHs and ERHs of all the mixtures in the levitation system demonstrated a smaller degree of reaction between MBTCA and NaCl compared to those obtained in the see-through impactor, which might be caused by the relatively closed atmosphere in the levitator as the default settings of $N_2$ flow inside the see-through impactor cell and the levitation cell were 4 and 0.2 $L \cdot min^{-1}$, respectively, i.e., less release of HCl. The larger size of the levitated particles could limit the release of HCl (Kerminen et al., 1997). In addition, the quenching process, i.e., the starting point of the hygroscopicity experiments, induced the solidification of MBTCA, and further, a slow reaction between MBTCA and NaCl.

## 4. Conclusions and atmospheric implication

The hygroscopic behavior, physical states, and chemical reactivity of pure MBTCA particles, mono-/di-/tri-sodium MBTCA salt particles, and MBTCA-NaCl particles of different mixing ratios were examined by in situ RMS assembled with a see-through impactor as the starting point with dehydration. The DRHs and ERHs of the laboratory-generated particles in the micrometer size range at room temperature were determined by monitoring the change in the particle area in the 2-D optical images and the corresponding Raman spectra at transition points with RH variation of ~1-95%. Pure MBTCA showed

three types of hygroscopic behaviors in that types 1 and 2 particles effloresced suddenly and gradually, respectively, at ERH = 30-58% during the dehydration process, whereas type 3 particles crystallized during the humidification process at RH = ~37%, not during the dehydration process because of a kinetic barrier to nucleation with limited condensed water. Subsequently, all particles maintained their crystal structure until RH = 95%. The mono- and di-sodium MBTCA salt aerosols did not show a clear ERH and DRH during the dehydration and humidification processes, respectively. In contrast, the tri-sodium MBTCA showed ERH = ~44.4-46.8% (during humidification) and DRH = ~53.1%. The MBTCA-NaCl droplets with molar mixing ratios of MBTCA:NaCl = 1:1 and 2:1 showed no distinct DRH and ERH because of the partial and complete reactions with NaCl, respectively, whereas those with ratios of MBTCA:NaCl =1:2 and 1:3 experienced single-stage efflorescence and deliquescence governed by the excess NaCl. Only monosodium MBTCA ($NaH_2M$) could be formed as a result of the reaction between NaCl and MBTCA regardless of the mixing ratios, mostly during the dehydration process within the timescale of one to two hours according to Raman analysis, indicating that the MBTCA-NaCl mixture systems are in an MBTCA-$NaH_2M$-NaCl ternary system except when NaCl has reacted completely in the mixture aerosols of MBTCA:NaCl = 2:1 ratio. The MBTCA-$NaH_2M$ existed as amorphous solids, even when the excess crystalline NaCl acted as a heterogeneous nucleation core, which was also confirmed by X-ray mapping. The reaction occurred more rapidly with a more elevated concentration of either MBTCA or NaCl, and the controlling factor for the reactivity of the mixtures depended mostly on the availability of $H^+$ dissociated from the MBTCA tricarboxylic acid. The hygroscopic experiments for pure MBTCA and MBTCA-NaCl mixture particles were also performed in a levitation system with the starting point from humidification after the quenching process and the RH variation of ~10 to 80%. The results acquired from the levitation system are consistent with those obtained from the see-through impactor, only with less reaction between MBTCA and NaCl resulting from the airtight atmosphere inside the levitator and the partial solidification of MBTCA after the quenching process. In addition, the elevated NaCl moiety can eventually transform the solidified MBTCA into droplets through reactions when absorbing adequate moisture.

These observations are expected to have important atmospheric implications in that they may help to better understand the complexity of real ambient SOA and inorganic mixture particles. In this study, the

hygroscopicity of MBTCA was altered significantly when mixed with NaCl due to the reaction, so that they are more likely to contribute to further gas-particle interactions. The amorphous phase state may influence the uptake of gaseous photo-oxidants as well as the chemical transformation and aging of atmospheric aerosols (Mikhailov et al., 2009). The observed aqueous shell with the solid core upon the humidification of the mixture particles with mixing ratios of MBTCA:NaCl = 1:2 and 1:3 before the total dissolution of NaCl can scatter solar radiation more efficiently (Adachi et al., 2011; Sun et al., 2018). The aerosol liquid water can promote heterogeneous aqueous-phase chemical processes, resulting in the facile formation of secondary aerosols (Cheng et al., 2016; Li et al., 2019). Recently, heterogeneous reactions in aerosol water were reported to be a significant mechanism for haze formation in North China (Sun et al., 2018). Overall, the hygroscopic curve, Raman signatures, and X-ray maps of the effloresced particles provided clear features of the hygroscopic behavior and chemical reactivity of the MBTCA-NaCl mixture system covered in this study. These results are expected to provide insights into the physicochemical characteristics and atmospheric chemistry of highly oxidized SOAs mixed with inorganic particles.

*Data availability.* The data used in this study are available upon request; please contact Chul-Un Ro (curo@inha.ac.kr).

*Author contributions.* LW, CB, SS, and CR designed the experiment. LW, CB, and SS carried out the measurements and/or analyzed the data. LW, CB, SS, PF, EP, EV, YS and CR contributed discussion of the data. LW, SS, and CR drafted the paper.

*Competing interests.* The authors declare that they have no conflict of interest.

*Acknowledgments.* This study was supported by Basic Science Research Programs through the National Research Foundation of Korea (NRF) funded by the Ministry of Education, Science, and Technology (NRF-2018R1A2A1A05023254) and by the National Strategic Project-Fine particle of the National Research Foundation of Korea (NRF) funded by the Ministry of Science and ICT (MSIT), the Ministry of Environment (ME), and the Ministry of Health and Welfare (MOHW) (2017M3D8A1090654).

Authors thank the Region Nouvelle Aquitaine for the financial support of the SPECAERO project. This work was performed through international and collaborative programs supported by PHC STAR n° 38815XE and visiting scholars program from IDEX of the University of Bordeaux.

## References

Adachi, K., Freney, E. J., and Buseck, P. R.: Shapes of internally mixed hygroscopic aerosol particles after deliquescence, and their effect on light scattering, Geophysical Research Letters, 38, n/a-n/a, 10.1029/2011gl047540, 2011.

Ahn, K.-H., Kim, S.-M., Jung, H.-J., Lee, M.-J., Eom, H.-J., Maskey, S., and Ro, C.-U.: Combined use of optical and electron microscopic techniques for the measurement of hygroscopic property, chemical composition, and morphology of individual aerosol particles, Analytical chemistry, 82, 7999-8009, 2010.

Aljawhary, D., Zhao, R., Lee, A. K., Wang, C., and Abbatt, J. P.: Kinetics, Mechanism, and Secondary Organic Aerosol Yield of Aqueous Phase Photo-oxidation of alpha-Pinene Oxidation Products, J Phys Chem A, 120, 1395-1407, 10.1021/acs.jpca.5b06237, 2016.

An, P., Yuan, C.-Q., Liu, X.-H., Xiao, D.-B., and Luo, Z.-X.: Vibrational spectroscopic identification of isoprene, pinenes and their mixture, Chinese Chemical Letters, 27, 527-534, 10.1016/j.cclet.2016.01.036, 2016.

Bateman, A. P., Bertram, A. K., and Martin, S. T.: Hygroscopic influence on the semisolid-to-liquid transition of secondary organic materials, J Phys Chem A, 119, 4386-4395, 10.1021/jp508521c, 2015a.

Bateman, A. P., Gong, Z., Liu, P., Sato, B., Cirino, G., Zhang, Y., Artaxo, P., Bertram, A. K., Manzi, A. O., Rizzo, L. V., Souza, R. A. F., Zaveri, R. A., and Martin, S. T.: Sub-micrometre particulate matter is primarily in liquid form over Amazon rainforest, Nature Geoscience, 9, 34-37, 10.1038/ngeo2599, 2015b.

Berkemeier, T., Shiraiwa, M., Pöschl, U., and Koop, T.: Competition between water uptake and ice nucleation by glassy organic aerosol particles, Atmospheric Chemistry and Physics, 14, 12513-12531, 10.5194/acp-14-12513-2014, 2014.

Bernard, F., Ciuraru, R., Boreave, A., and George, C.: Photosensitized Formation of Secondary Organic Aerosols above the Air/Water Interface, Environ Sci Technol, 50, 8678-8686, 10.1021/acs.est.6b03520, 2016.

Bertran, O., Armelin, E., Estrany, F., Gomes, A., Torras, J., and Alemán, C.: Poly (2-thiophen-3-yl-malonic acid), a polythiophene with two carboxylic acids per repeating unit, The Journal of Physical Chemistry B, 114, 6281-6290, 2010.

Cheng, Y., Zheng, G., Wei, C., Mu, Q., Zheng, B., Wang, Z., Gao, M., Zhang, Q., He, K., and Carmichael, G.: Reactive nitrogen chemistry in aerosol water as a source of sulfate during haze events in China, Science Advances, 2, e1601530, 2016.

Chu, B., Wang, K., Takekawa, H., Li, J., Zhou, W., Jiang, J., Ma, Q., He, H., and Hao, J.: Hygroscopicity of particles generated from photooxidation of α-pinene under different oxidation conditions in the

712 presence of sulfate seed aerosols, Journal of Environmental Sciences, 26, 129-139,
713 10.1016/s1001-0742(13)60402-7, 2014.
714 Clegg, S. L., Seinfeld, J. H., and Edney, E. O.: Thermodynamic modelling of aqueous aerosols containing
715 electrolytes and dissolved organic compounds. II. An extended Zdanovskii–Stokes–Robinson
716 approach, Journal of aerosol science, 34, 667-690, 2003.
717 Cui, T., Green, H. S., Selleck, P. W., Zhang, Z., O'Brien, R. E., Gold, A., Keywood, M., Kroll, J. H., and
718 Surratt, J. D.: Chemical Characterization of Isoprene- and Monoterpene-Derived Secondary
719 Organic Aerosol Tracers in Remote Marine Aerosols over a Quarter Century, ACS Earth and
720 Space Chemistry, 3, 935-946, 10.1021/acsearthspacechem.9b00061, 2019.
721 Dette, H. P., Qi, M., Schroder, D. C., Godt, A., and Koop, T.: Glass-forming properties of 3-
722 methylbutane-1,2,3-tricarboxylic acid and its mixtures with water and pinonic acid, J Phys Chem
723 A, 118, 7024-7033, 10.1021/jp505910w, 2014.
724 Ding, X., Wang, X.-M., Gao, B., Fu, X.-X., He, Q.-F., Zhao, X.-Y., Yu, J.-Z., and Zheng, M.: Tracer-
725 based estimation of secondary organic carbon in the Pearl River Delta, south China, Journal of
726 Geophysical Research: Atmospheres, 117, n/a-n/a, 10.1029/2011jd016596, 2012.
727 Donahue, N. M., Henry, K. M., Mentel, T. F., Kiendler-Scharr, A., Spindler, C., Bohn, B., Brauers, T.,
728 Dorn, H. P., Fuchs, H., Tillmann, R., Wahner, A., Saathoff, H., Naumann, K. H., Mohler, O.,
729 Leisner, T., Muller, L., Reinnig, M. C., Hoffmann, T., Salo, K., Hallquist, M., Frosch, M., Bilde,
730 M., Tritscher, T., Barmet, P., Praplan, A. P., DeCarlo, P. F., Dommen, J., Prevot, A. S., and
731 Baltensperger, U.: Aging of biogenic secondary organic aerosol via gas-phase OH radical
732 reactions, Proc Natl Acad Sci U S A, 109, 13503-13508, 10.1073/pnas.1115186109, 2012.
733 Dunne, E. M., Gordon, H., Kurten, A., Almeida, J., Duplissy, J., Williamson, C., Ortega, I. K., Pringle,
734 K. J., Adamov, A., Baltensperger, U., Barmet, P., Benduhn, F., Bianchi, F., Breitenlechner, M.,
735 Clarke, A., Curtius, J., Dommen, J., Donahue, N. M., Ehrhart, S., Flagan, R. C., Franchin, A.,
736 Guida, R., Hakala, J., Hansel, A., Heinritzi, M., Jokinen, T., Kangasluoma, J., Kirkby, J., Kulmala,
737 M., Kupc, A., Lawler, M. J., Lehtipalo, K., Makhmutov, V., Mann, G., Mathot, S., Merikanto, J.,
738 Miettinen, P., Nenes, A., Onnela, A., Rap, A., Reddington, C. L., Riccobono, F., Richards, N. A.,
739 Rissanen, M. P., Rondo, L., Sarnela, N., Schobesberger, S., Sengupta, K., Simon, M., Sipila, M.,
740 Smith, J. N., Stozkhov, Y., Tome, A., Trostl, J., Wagner, P. E., Wimmer, D., Winkler, P. M.,
741 Worsnop, D. R., and Carslaw, K. S.: Global atmospheric particle formation from CERN CLOUD
742 measurements, Science, 354, 1119-1124, 10.1126/science.aaf2649, 2016.
743 Edsall, J. T.: Raman Spectra of Amino Acids and Related Compounds IV. Ionization of Di- and
744 Tricarboxylic Acids, The Journal of Chemical Physics, 5, 508-517, 10.1063/1.1750067, 1937.
745 Enami, S., and Sakamoto, Y.: OH-Radical Oxidation of Surface-Active cis-Pinonic Acid at the Air-Water
746 Interface, J Phys Chem A, 120, 3578-3587, 10.1021/acs.jpca.6b01261, 2016.
747 Eom, H. J., Gupta, D., Li, X., Jung, H. J., Kim, H., and Ro, C. U.: Influence of collecting substrates on
748 the characterization of hygroscopic properties of inorganic aerosol particles, Anal Chem, 86,
749 2648-2656, 10.1021/ac4042075, 2014.
750 Freedman, M. A.: Phase separation in organic aerosol, Chemical Society Reviews, 46, 7694-7705, 2017.
751 Fu, P., Kawamura, K., Chen, J., and Barrie, L. A.: Isoprene, monoterpene, and sesquiterpene oxidation
752 products in the high Arctic aerosols during late winter to early summer, Environmental Science
753 & Technology, 43, 4022-4028, 2009.

Fu, P. Q., Kawamura, K., Cheng, Y. F., Hatakeyama, S., Takami, A., Li, H., and Wang, W.: Aircraft measurements of polar organic tracer compounds in tropospheric particles (PM<sub>10</sub>) over central China, Atmospheric Chemistry and Physics, 14, 4185-4199, 10.5194/acp-14-4185-2014, 2014.
Ge, Z., Wexler, A. S., and Johnston, M. V.: Multicomponent aerosol crystallization, Journal of Colloid and Interface Science, 183, 68-77, 1996.
Gibson, E. R., Hudson, P. K., and Grassian, V. H.: Physicochemical properties of nitrate aerosols: Implications for the atmosphere, The Journal of Physical Chemistry A, 110, 11785-11799, 2006.
Gómez-González, Y., Wang, W., Vermeylen, R., Chi, X., Neirynck, J., Janssens, I. A., Maenhaut, W., and Claeys, M.: Chemical characterisation of atmospheric aerosols during a 2007 summer field campaign at Brasschaat, Belgium: sources and source processes of biogenic secondary organic aerosol, Atmospheric Chemistry and Physics, 12, 125-138, 10.5194/acp-12-125-2012, 2012.
Guenther, A., Hewitt, C. N., Erickson, D., Fall, R., Geron, C., Graedel, T., Harley, P., Klinger, L., Lerdau, M., and McKay, W.: A global model of natural volatile organic compound emissions, Journal of Geophysical Research: Atmospheres, 100, 8873-8892, 1995.
Gupta, D., Eom, H. J., Cho, H. R., and Ro, C. U.: Hygroscopic behavior of NaCl–MgCl2 mixture particles as nascent sea-spray aerosol surrogates and observation of efflorescence during humidification, Atmospheric Chemistry and Physics, 15, 11273-11290, 10.5194/acp-15-11273-2015, 2015.
Gysel, M., Weingartner, E., and Baltensperger, U.: Hygroscopicity of aerosol particles at low temperatures. 2. Theoretical and experimental hygroscopic properties of laboratory generated aerosols, Environmental science & technology, 36, 63-68, 2002.
Hallquist, M., Wenger, J. C., Baltensperger, U., Rudich, Y., Simpson, D., Claeys, M., Dommen, J., Donahue, N., George, C., and Goldstein, A.: The formation, properties and impact of secondary organic aerosol: current and emerging issues, Atmospheric chemistry and physics, 9, 5155-5236, 2009.
Harris, D. C.: Exploring chemical analysis, Macmillan, 2012.
Haywood, J., and Boucher, O.: Estimates of the direct and indirect radiative forcing due to tropospheric aerosols: A review, Reviews of geophysics, 38, 513-543, 2000.
Hoffman, R. C., Laskin, A., and Finlayson-Pitts, B. J.: Sodium nitrate particles: physical and chemical properties during hydration and dehydration, and implications for aged sea salt aerosols, Journal of Aerosol Science, 35, 869-887, 10.1016/j.jaerosci.2004.02.003, 2004.
Holopainen, J. K., Kivimaenpaa, M., and Nizkorodov, S. A.: Plant-derived Secondary Organic Material in the Air and Ecosystems, Trends Plant Sci, 22, 744-753, 10.1016/j.tplants.2017.07.004, 2017.
Hong, Z., Zhang, H., Zhang, Y., Xu, L., Liu, T., Xiao, H., Hong, Y., Chen, J., Li, M., Deng, J., Wu, X., Hu, B., and Chen, X.: Secondary organic aerosol of PM2.5 in a mountainous forest area in southeastern China: Molecular compositions and tracers implication, Sci Total Environ, 653, 496-503, 10.1016/j.scitotenv.2018.10.370, 2019.
Hu, D., Bian, Q., Li, T. W. Y., Lau, A. K. H., and Yu, J. Z.: Contributions of isoprene, monoterpenes,β-caryophyllene, and toluene to secondary organic aerosols in Hong Kong during the summer of 2006, Journal of Geophysical Research, 113, 10.1029/2008jd010437, 2008.

Hu, Q. H., Xie, Z. Q., Wang, X. M., Kang, H., He, Q. F., and Zhang, P.: Secondary organic aerosols over oceans via oxidation of isoprene and monoterpenes from Arctic to Antarctic, Sci Rep, 3, 2280, 10.1038/srep02280, 2013.
Jang, M., Czoschke, N. M., Lee, S., and Kamens, R. M.: Heterogeneous atmospheric aerosol production by acid-catalyzed particle-phase reactions, Science, 298, 814-817, 2002.
Jaoui, M., Kleindienst, T., Lewandowski, M., Offenberg, J., and Edney, E.: Identification and quantification of aerosol polar oxygenated compounds bearing carboxylic or hydroxyl groups. 2. Organic tracer compounds from monoterpenes, Environmental science & technology, 39, 5661-5673, 2005.
Jimenez, J. L., Canagaratna, M., Donahue, N., Prevot, A., Zhang, Q., Kroll, J. H., DeCarlo, P. F., Allan, J. D., Coe, H., and Ng, N.: Evolution of organic aerosols in the atmosphere, science, 326, 1525-1529, 2009.
Jing, B., Tong, S., Liu, Q., Li, K., Wang, W., Zhang, Y., and Ge, M.: Hygroscopic behavior of multicomponent organic aerosols and their internal mixtures with ammonium sulfate, Atmospheric Chemistry and Physics, 16, 4101-4118, 10.5194/acp-16-4101-2016, 2016.
Jing, B., Wang, Z., Tan, F., Guo, Y., Tong, S., Wang, W., Zhang, Y., and Ge, M.: Hygroscopic behavior of atmospheric aerosols containing nitrate salts and water-soluble organic acids, Atmospheric Chemistry and Physics, 18, 5115-5127, 10.5194/acp-18-5115-2018, 2018.
Kammer, J., Perraudin, E., Flaud, P. M., Lamaud, E., Bonnefond, J. M., and Villenave, E.: Observation of nighttime new particle formation over the French Landes forest, Sci Total Environ, 621, 1084-1092, 10.1016/j.scitotenv.2017.10.118, 2018.
Kang, M., Fu, P., Kawamura, K., Yang, F., Zhang, H., Zang, Z., Ren, H., Ren, L., Zhao, Y., Sun, Y., and Wang, Z.: Characterization of biogenic primary and secondary organic aerosols in the marine atmosphere over the East China Sea, Atmospheric Chemistry and Physics, 18, 13947-13967, 10.5194/acp-18-13947-2018, 2018.
Karadima, K. S., Mavrantzas, V. G., and Pandis, S. N.: Insights into the morphology of multicomponent organic and inorganic aerosols from molecular dynamics simulations, Atmospheric Chemistry and Physics, 19, 5571-5587, 10.5194/acp-19-5571-2019, 2019.
Kerminen, V.-M., Pakkanen, T. A., and Hillamo, R. E.: Interactions between inorganic trace gases and supermicrometer particles at a coastal site, Atmospheric Environment, 31, 2753-2765, 1997.
Kidd, C., Perraud, V., Wingen, L. M., and Finlayson-Pitts, B. J.: Integrating phase and composition of secondary organic aerosol from the ozonolysis of α-pinene, Proceedings of the National Academy of Sciences, 111, 7552-7557, 2014.
Kildgaard, J. V., Mikkelsen, K. V., Bilde, M., and Elm, J.: Hydration of Atmospheric Molecular Clusters II: Organic Acid-Water Clusters, J Phys Chem A, 122, 8549-8556, 10.1021/acs.jpca.8b07713, 2018.
Kim, H., Lee, M.-J., Jung, H.-J., Eom, H.-J., Maskey, S., Ahn, K.-H., and Ro, C.-U.: Hygroscopic behavior of wet dispersed and dry deposited NaNO3 particles, Atmospheric Environment, 60, 68-75, 10.1016/j.atmosenv.2012.06.011, 2012.
Kim, H., Zhang, Q., and Heo, J.: Influence of intense secondary aerosol formation and long-range transport on aerosol chemistry and properties in the Seoul Metropolitan Area during spring time:

results from KORUS-AQ, Atmospheric Chemistry and Physics, 18, 7149-7168, 10.5194/acp-18-7149-2018, 2018.
Koop, T., Bookhold, J., Shiraiwa, M., and Pöschl, U.: Glass transition and phase state of organic compounds: dependency on molecular properties and implications for secondary organic aerosols in the atmosphere, Physical Chemistry Chemical Physics, 13, 19238-19255, 2011.
Kostenidou, E., Karnezi, E., Kolodziejczyk, A., Szmigielski, R., and Pandis, S. N.: Physical and Chemical Properties of 3-Methyl-1,2,3-butanetricarboxylic Acid (MBTCA) Aerosol, Environ Sci Technol, 52, 1150-1155, 10.1021/acs.est.7b04348, 2018.
Kourtchev, I., Copolovici, L., Claeys, M., and Maenhaut, W.: Characterization of atmospheric aerosols at a forested site in Central Europe, Environmental science & technology, 43, 4665-4671, 2009.
Kroll, J. H., and Seinfeld, J. H.: Chemistry of secondary organic aerosol: Formation and evolution of low-volatility organics in the atmosphere, Atmospheric Environment, 42, 3593-3624, 2008.
Kubátová, A., Vermeylen, R., Claeys, M., Cafmeyer, J., Maenhaut, W., Roberts, G., and Artaxo, P.: Carbonaceous aerosol characterization in the Amazon basin, Brazil: novel dicarboxylic acids and related compounds, Atmospheric Environment, 34, 5037-5051, 2000.
Kubátová, A., Vermeylen, R., Claeys, M., Cafmeyer, J., and Maenhaut, W.: Organic compounds in urban aerosols from Gent, Belgium: Characterization, sources, and seasonal differences, Journal of Geophysical Research: Atmospheres, 107, ICC 5-1-ICC 5-12, 10.1029/2001jd000556, 2002.
Lai, C., Liu, Y., Ma, J., Ma, Q., Chu, B., and He, H.: Heterogeneous Kinetics of cis-Pinonic Acid with Hydroxyl Radical under Different Environmental Conditions, J Phys Chem A, 119, 6583-6593, 10.1021/acs.jpca.5b01321, 2015.
Laskin, A., Moffet, R. C., Gilles, M. K., Fast, J. D., Zaveri, R. A., Wang, B., Nigge, P., and Shutthanandan, J.: Tropospheric chemistry of internally mixed sea salt and organic particles: Surprising reactivity of NaCl with weak organic acids, Journal of Geophysical Research: Atmospheres, 117, n/a-n/a, 10.1029/2012jd017743, 2012.
Lee, A. K. Y., Ling, T. Y., and Chan, C. K.: Understanding hygroscopic growth and phase transformation of aerosols using single particle Raman spectroscopy in an electrodynamic balance, Faraday Discuss., 137, 245-263, 10.1039/b704580h, 2008.
Lessmeier, J., Dette, H. P., Godt, A., and Koop, T.: Physical state of 2-methylbutane-1,2,3,4-tetraol in pure and internally mixed aerosols, Atmospheric Chemistry and Physics, 18, 15841-15857, 10.5194/acp-18-15841-2018, 2018.
Li, J. J., Wang, G. H., Cao, J. J., Wang, X. M., and Zhang, R. J.: Observation of biogenic secondary organic aerosols in the atmosphere of a mountain site in central China: temperature and relative humidity effects, Atmospheric Chemistry and Physics, 13, 11535-11549, 10.5194/acp-13-11535-2013, 2013.
Li, X., Gupta, D., Eom, H.-J., Kim, H., and Ro, C.-U.: Deliquescence and efflorescence behavior of individual NaCl and KCl mixture aerosol particles, Atmospheric Environment, 82, 36-43, 10.1016/j.atmosenv.2013.10.011, 2014.
Li, X., Gupta, D., Lee, J., Park, G., and Ro, C. U.: Real-Time Investigation of Chemical Compositions and Hygroscopic Properties of Aerosols Generated from NaCl and Malonic Acid Mixture Solutions Using in Situ Raman Microspectrometry, Environ Sci Technol, 51, 263-270, 10.1021/acs.est.6b04356, 2017.

Li, X., Song, S., Zhou, W., Hao, J., Worsnop, D. R., and Jiang, J.: Interactions between aerosol organic components and liquid water content during haze episodes in Beijing, Atmospheric Chemistry and Physics, 19, 12163-12174, 10.5194/acp-19-12163-2019, 2019.

Lightstone, J. M., Onasch, T. B., Imre, D., and Oatis, S.: Deliquescence, efflorescence, and water activity in ammonium nitrate and mixed ammonium nitrate/succinic acid microparticles, The Journal of Physical Chemistry A, 104, 9337-9346, 2000.

Lignell, H., Epstein, S. A., Marvin, M. R., Shemesh, D., Gerber, B., and Nizkorodov, S.: Experimental and theoretical study of aqueous cis-pinonic acid photolysis, J Phys Chem A, 117, 12930-12945, 10.1021/jp4093018, 2013.

Liu, T., Zhou, L., Liu, Q., Lee, B. P., Yao, D., Lu, H., Lyu, X., Guo, H., and Chan, C. K.: Secondary Organic Aerosol Formation from Urban Roadside Air in Hong Kong, Environ Sci Technol, 53, 3001-3009, 10.1021/acs.est.8b06587, 2019.

Ma, Q., Ma, J., Liu, C., Lai, C., and He, H.: Laboratory study on the hygroscopic behavior of external and internal C2-C4 dicarboxylic acid-NaCl mixtures, Environ Sci Technol, 47, 10381-10388, 10.1021/es4023267, 2013.

Marsh, A., Rovelli, G., Miles, R. E. H., and Reid, J. P.: Complexity of Measuring and Representing the Hygroscopicity of Mixed Component Aerosol, J Phys Chem A, 123, 1648-1660, 10.1021/acs.jpca.8b11623, 2019.

Martin, S. T.: Phase transitions of aqueous atmospheric particles, Chemical Reviews, 100, 3403-3454, 2000.

Mikhailov, E., Vlasenko, S., Martin, S., Koop, T., and Pöschl, U.: Amorphous and crystalline aerosol particles interacting with water vapor: conceptual framework and experimental evidence for restructuring, phase transitions and kinetic limitations, Atmospheric Chemistry and Physics, 9, 9491-9522, 2009.

Miyazaki, Y., Jung, J., Fu, P., Mizoguchi, Y., Yamanoi, K., and Kawamura, K.: Evidence of formation of submicrometer water-soluble organic aerosols at a deciduous forest site in northern Japan in summer, Journal of Geophysical Research: Atmospheres, 117, n/a-n/a, 10.1029/2012jd018250, 2012.

Müller, L., Reinnig, M. C., Naumann, K. H., Saathoff, H., Mentel, T. F., Donahue, N. M., and Hoffmann, T.: Formation of 3-methyl-1,2,3-butanetricarboxylic acid via gas phase oxidation of pinonic acid – a mass spectrometric study of SOA aging, Atmospheric Chemistry and Physics, 12, 1483-1496, 10.5194/acp-12-1483-2012, 2012.

Mutzel, A., Rodigast, M., Iinuma, Y., Böge, O., and Herrmann, H.: Monoterpene SOA–contribution of first-generation oxidation products to formation and chemical composition, Atmospheric environment, 130, 136-144, 2016.

Pajunoja, A., Hu, W., Leong, Y. J., Taylor, N. F., Miettinen, P., Palm, B. B., Mikkonen, S., Collins, D. R., Jimenez, J. L., and Virtanen, A.: Phase state of ambient aerosol linked with water uptake and chemical aging in the southeastern US, Atmospheric Chemistry and Physics, 16, 11163-11176, 2016.

Parsons, M. T., Knopf, D. A., and Bertram, A. K.: Deliquescence and Crystallization of Ammonium Sulfate Particles Internally Mixed with Water-Soluble Organic Compounds, The Journal of Physical Chemistry A, 108, 11600-11608, 10.1021/jp0462862, 2004.

Pöhlker, C., Saturno, J., Krüger, M. L., Förster, J.-D., Weigand, M., Wiedemann, K. T., Bechtel, M., Artaxo, P., and Andreae, M. O.: Efflorescence upon humidification? X-ray microspectroscopic in situ observation of changes in aerosol microstructure and phase state upon hydration, Geophysical Research Letters, 41, 3681-3689, 10.1002/2014gl059409, 2014.

Poschl, U., and Shiraiwa, M.: Multiphase chemistry at the atmosphere-biosphere interface influencing climate and public health in the anthropocene, Chem Rev, 115, 4440-4475, 10.1021/cr500487s, 2015.

Praplan, A. P., Barmet, P., Dommen, J., and Baltensperger, U.: Cyclobutyl methyl ketone as a model compound for pinonic acid to elucidate oxidation mechanisms, Atmospheric Chemistry and Physics, 12, 10749-10758, 10.5194/acp-12-10749-2012, 2012.

Reid, J. P., Bertram, A. K., Topping, D. O., Laskin, A., Martin, S. T., Petters, M. D., Pope, F. D., and Rovelli, G.: The viscosity of atmospherically relevant organic particles, Nat Commun, 9, 956, 10.1038/s41467-018-03027-z, 2018.

Renbaum-Wolff, L., Grayson, J. W., Bateman, A. P., Kuwata, M., Sellier, M., Murray, B. J., Shilling, J. E., Martin, S. T., and Bertram, A. K.: Viscosity of alpha-pinene secondary organic material and implications for particle growth and reactivity, Proc Natl Acad Sci U S A, 110, 8014-8019, 10.1073/pnas.1219548110, 2013.

Rudich, Y., Donahue, N. M., and Mentel, T. F.: Aging of organic aerosol: Bridging the gap between laboratory and field studies, Annual Review of Physical Chemistry, 58, 321-352, 10.1146/annurev.physchem.58.032806.104432, 2007.

Sato, K., Jia, T., Tanabe, K., Morino, Y., Kajii, Y., and Imamura, T.: Terpenylic acid and nine-carbon multifunctional compounds formed during the aging of β-pinene ozonolysis secondary organic aerosol, Atmospheric Environment, 130, 127-135, 10.1016/j.atmosenv.2015.08.047, 2016.

Saukko, E., Lambe, A. T., Massoli, P., Koop, T., Wright, J. P., Croasdale, D. R., Pedernera, D. A., Onasch, T. B., Laaksonen, A., Davidovits, P., Worsnop, D. R., and Virtanen, A.: Humidity-dependent phase state of SOA particles from biogenic and anthropogenic precursors, Atmospheric Chemistry and Physics, 12, 7517-7529, 10.5194/acp-12-7517-2012, 2012.

Schlenker, J. C., and Martin, S. T.: Crystallization pathways of sulfate− nitrate− ammonium aerosol particles, The Journal of Physical Chemistry A, 109, 9980-9985, 2005.

Seaver, M., Galloway, A., and Manuccia, T. J.: Acoustic levitation in a free-jet wind tunnel, Review of Scientific Instruments, 60, 3452-3459, 10.1063/1.1140492, 1989.

Seng, S., Guo, F., Tobon, Y. A., Ishikawa, T., Moreau, M., Ishizaka, S., and Sobanska, S.: Deliquescence behavior of photo-irradiated single NaNO3 droplets, Atmospheric Environment, 183, 33-39, 10.1016/j.atmosenv.2018.04.007, 2018.

Shiraiwa, M., Li, Y., Tsimpidi, A. P., Karydis, V. A., Berkemeier, T., Pandis, S. N., Lelieveld, J., Koop, T., and Poschl, U.: Global distribution of particle phase state in atmospheric secondary organic aerosols, Nat Commun, 8, 15002, 10.1038/ncomms15002, 2017.

Shrivastava, M., Easter, R. C., Liu, X., Zelenyuk, A., Singh, B., Zhang, K., Ma, P.-L., Chand, D., Ghan, S., Jimenez, J. L., Zhang, Q., Fast, J., Rasch, P. J., and Tiitta, P.: Global transformation and fate of SOA: Implications of low-volatility SOA and gas-phase fragmentation reactions, Journal of Geophysical Research: Atmospheres, 120, 4169-4195, 10.1002/2014jd022563, 2015.

960 Shrivastava, M., Cappa, C. D., Fan, J., Goldstein, A. H., Guenther, A. B., Jimenez, J. L., Kuang, C.,
961 Laskin, A., Martin, S. T., Ng, N. L., Petaja, T., Pierce, J. R., Rasch, P. J., Roldin, P., Seinfeld, J.
962 H., Shilling, J., Smith, J. N., Thornton, J. A., Volkamer, R., Wang, J., Worsnop, D. R., Zaveri, R.
963 A., Zelenyuk, A., and Zhang, Q.: Recent advances in understanding secondary organic aerosol:
964 Implications for global climate forcing, Reviews of Geophysics, 55, 509-559,
965 10.1002/2016rg000540, 2017.
966 Slade, J. H., Ault, A. P., Bui, A. T., Ditto, J. C., Lei, Z., Bondy, A. L., Olson, N. E., Cook, R. D.,
967 Desrochers, S. J., Harvey, R. M., Erickson, M. H., Wallace, H. W., Alvarez, S. L., Flynn, J. H.,
968 Boor, B. E., Petrucci, G. A., Gentner, D. R., Griffin, R. J., and Shepson, P. B.: Bouncier Particles
969 at Night: Biogenic Secondary Organic Aerosol Chemistry and Sulfate Drive Diel Variations in
970 the Aerosol Phase in a Mixed Forest, Environ Sci Technol, 53, 4977-4987,
971 10.1021/acs.est.8b07319, 2019.
972 Song, M., Maclean, A. M., Huang, Y., Smith, N. R., Blair, S. L., Laskin, J., Laskin, A., DeRieux, W.-S.
973 W., Li, Y., Shiraiwa, M., Nizkorodov, S. A., and Bertram, A. K.: Liquid–liquid phase separation
974 and viscosity within secondary organic aerosol generated from diesel fuel vapors, Atmospheric
975 Chemistry and Physics, 19, 12515-12529, 10.5194/acp-19-12515-2019, 2019.
976 Song, Y. C., Haddrell, A. E., Bzdek, B. R., Reid, J. P., Bannan, T., Topping, D. O., Percival, C., and Cai,
977 C.: Measurements and predictions of binary component aerosol particle viscosity, The Journal of
978 Physical Chemistry A, 120, 8123-8137, 2016.
979 Srivastava, D., Favez, O., Perraudin, E., Villenave, E., and Albinet, A.: Comparison of Measurement-
980 Based Methodologies to Apportion Secondary Organic Carbon (SOC) in PM2.5: A Review of
981 Recent Studies, Atmosphere, 9, 10.3390/atmos9110452, 2018.
982 Sun, J., Liu, L., Xu, L., Wang, Y., Wu, Z., Hu, M., Shi, Z., Li, Y., Zhang, X., Chen, J., and Li, W.: Key
983 Role of Nitrate in Phase Transitions of Urban Particles: Implications of Important Reactive
984 Surfaces for Secondary Aerosol Formation, Journal of Geophysical Research: Atmospheres, 123,
985 1234-1243, 10.1002/2017jd027264, 2018.
986 Szmigielski, R., Surratt, J. D., Gómez-González, Y., Van der Veken, P., Kourtchev, I., Vermeylen, R.,
987 Blockhuys, F., Jaoui, M., Kleindienst, T. E., Lewandowski, M., Offenberg, J. H., Edney, E. O.,
988 Seinfeld, J. H., Maenhaut, W., and Claeys, M.: 3-methyl-1,2,3-butanetricarboxylic acid: An
989 atmospheric tracer for terpene secondary organic aerosol, Geophysical Research Letters, 34,
990 10.1029/2007gl031338, 2007.
991 Tang, M., Chan, C. K., Li, Y. J., Su, H., Ma, Q., Wu, Z., Zhang, G., Wang, Z., Ge, M., Hu, M., He, H.,
992 and Wang, X.: A review of experimental techniques for aerosol hygroscopicity studies,
993 Atmospheric Chemistry and Physics, 19, 12631-12686, 10.5194/acp-19-12631-2019, 2019.
994 Topping, D., Connolly, P., and McFiggans, G.: Cloud droplet number enhanced by co-condensation of
995 organic vapours, Nature Geoscience, 6, 443, 2013.
996 Virtanen, A., Joutsensaari, J., Koop, T., Kannosto, J., Yli-Pirilä, P., Leskinen, J., Mäkelä, J. M.,
997 Holopainen, J. K., Pöschl, U., and Kulmala, M.: An amorphous solid state of biogenic secondary
998 organic aerosol particles, Nature, 467, 824, 2010.
999 Vlachou, A., Tobler, A., Lamkaddam, H., Canonaco, F., Daellenbach, K. R., Jaffrezo, J.-L., Minguillón,
1000 M. C., Maasikmets, M., Teinemaa, E., Baltensperger, U., El Haddad, I., and Prévôt, A. S. H.:
1001 Development of a versatile source apportionment analysis based on positive matrix factorization:

a case study of the seasonal variation of organic aerosol sources in Estonia, Atmospheric Chemistry and Physics, 19, 7279-7295, 10.5194/acp-19-7279-2019, 2019.
Vogel, A. L., Äijälä, M., Corrigan, A. L., Junninen, H., Ehn, M., Petäjä, T., Worsnop, D. R., Kulmala, M., Russell, L. M., Williams, J., and Hoffmann, T.: In situ submicron organic aerosol characterization at a boreal forest research station during HUMPPA-COPEC 2010 using soft and hard ionization mass spectrometry, Atmospheric Chemistry and Physics, 13, 10933-10950, 10.5194/acp-13-10933-2013, 2013.
Wang, B., O'Brien, R. E., Kelly, S. T., Shilling, J. E., Moffet, R. C., Gilles, M. K., and Laskin, A.: Reactivity of liquid and semisolid secondary organic carbon with chloride and nitrate in atmospheric aerosols, J Phys Chem A, 119, 4498-4508, 10.1021/jp510336q, 2015.
Wang, X., Jing, B., Tan, F., Ma, J., Zhang, Y., and Ge, M.: Hygroscopic behavior and chemical composition evolution of internally mixed aerosols composed of oxalic acid and ammonium sulfate, Atmospheric Chemistry and Physics, 17, 12797-12812, 10.5194/acp-17-12797-2017, 2017.
Wang, Z., Jing, B., Shi, X., Tong, S., Wang, W., and Ge, M.: Importance of water-soluble organic acid on the hygroscopicity of nitrate, Atmospheric Environment, 190, 65-73, 10.1016/j.atmosenv.2018.07.010, 2018.
Wu, L., Li, X., Kim, H., Geng, H., Godoi, R. H. M., Barbosa, C. G. G., Godoi, A. F. L., Yamamoto, C. I., de Souza, R. A. F., Pöhlker, C., Andreae, M. O., and Ro, C.-U.: Single-particle characterization of aerosols collected at a remote site in the Amazonian rainforest and an urban site in Manaus, Brazil, Atmospheric Chemistry and Physics, 19, 1221-1240, 10.5194/acp-19-1221-2019, 2019a.
Wu, L., Li, X., and Ro, C.-U.: Hygroscopic Behavior of Ammonium Sulfate, Ammonium Nitrate, and their Mixture Particles, Asian Journal of Atmospheric Environment, 13, 196-211, 10.5572/ajae.2019.13.3.196, 2019b.
Wu, L., and Ro, C.-U.: Aerosol Hygroscopicity on A Single Particle Level Using Microscopic and Spectroscopic Techniques: A Review, Asian Journal of Atmospheric Environment, 14, 177-209, 10.5572/ajae.2020.14.3.177, 2020.
Wu, Z. J., Nowak, A., Poulain, L., Herrmann, H., and Wiedensohler, A.: Hygroscopic behavior of atmospherically relevant water-soluble carboxylic salts and their influence on the water uptake of ammonium sulfate, Atmospheric Chemistry and Physics, 11, 12617-12626, 10.5194/acp-11-12617-2011, 2011.
Yasmeen, F., Szmigielski, R., Vermeylen, R., Gomez-Gonzalez, Y., Surratt, J. D., Chan, A. W., Seinfeld, J. H., Maenhaut, W., and Claeys, M.: Mass spectrometric characterization of isomeric terpenoic acids from the oxidation of alpha-pinene, beta-pinene, d-limonene, and Delta3-carene in fine forest aerosol, J Mass Spectrom, 46, 425-442, 10.1002/jms.1911, 2011.
Yatavelli, R. L. N., Mohr, C., Stark, H., Day, D. A., Thompson, S. L., Lopez-Hilfiker, F. D., Campuzano-Jost, P., Palm, B. B., Vogel, A. L., Hoffmann, T., Heikkinen, L., Äijälä, M., Ng, N. L., Kimmel, J. R., Canagaratna, M. R., Ehn, M., Junninen, H., Cubison, M. J., Petäjä, T., Kulmala, M., Jayne, J. T., Worsnop, D. R., and Jimenez, J. L.: Estimating the contribution of organic acids to northern hemispheric continental organic aerosol, Geophysical Research Letters, 42, 6084-6090, 10.1002/2015gl064650, 2015.

Zhang, Y. Y., Müller, L., Winterhalter, R., Moortgat, G. K., Hoffmann, T., and Pöschl, U.: Seasonal cycle and temperature dependence of pinene oxidation products, dicarboxylic acids and nitrophenols in fine and coarse air particulate matter, Atmospheric Chemistry and Physics, 10, 7859-7873, 10.5194/acp-10-7859-2010, 2010.

Figure 1. Calculated titration curve for MBTCA, noted as $H_3M$ in this figure. The experimental data are shown as orange triangles. 5 mL of 0.02 M $H_3M$ was titrated with a 0.1 M NaOH solution.

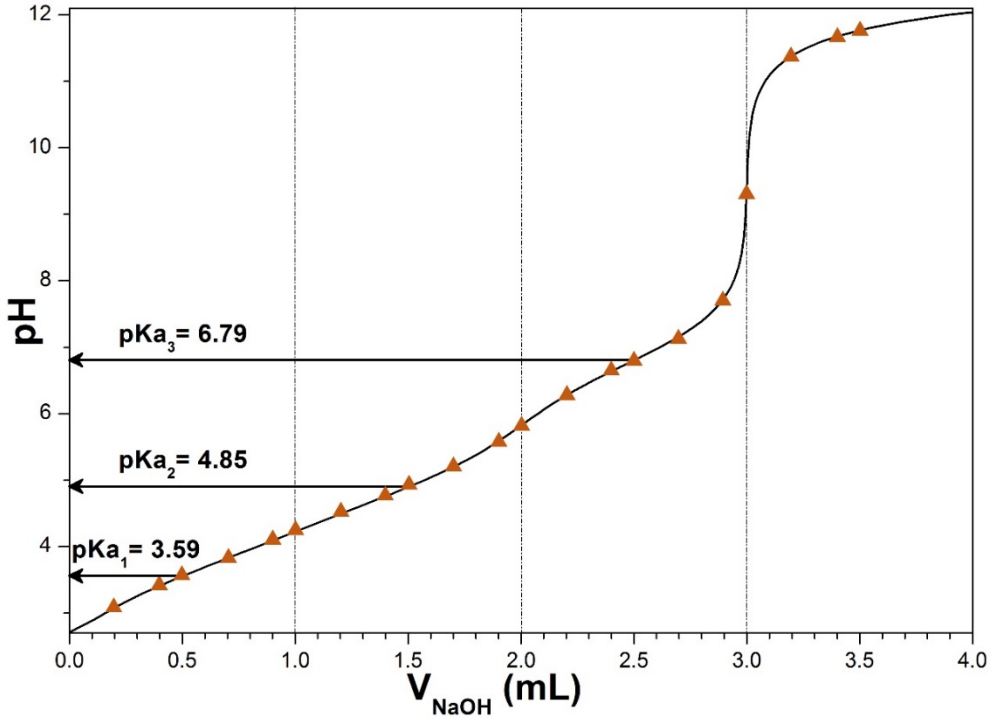

Figure 2. Hygroscopic curves, corresponding optical images, and Raman spectra at specific RHs of three types of pure MBTCA particles. The transition RHs recorded during the dehydration (D) and humidification (H) processes are marked with arrows in the hygroscopic curves.

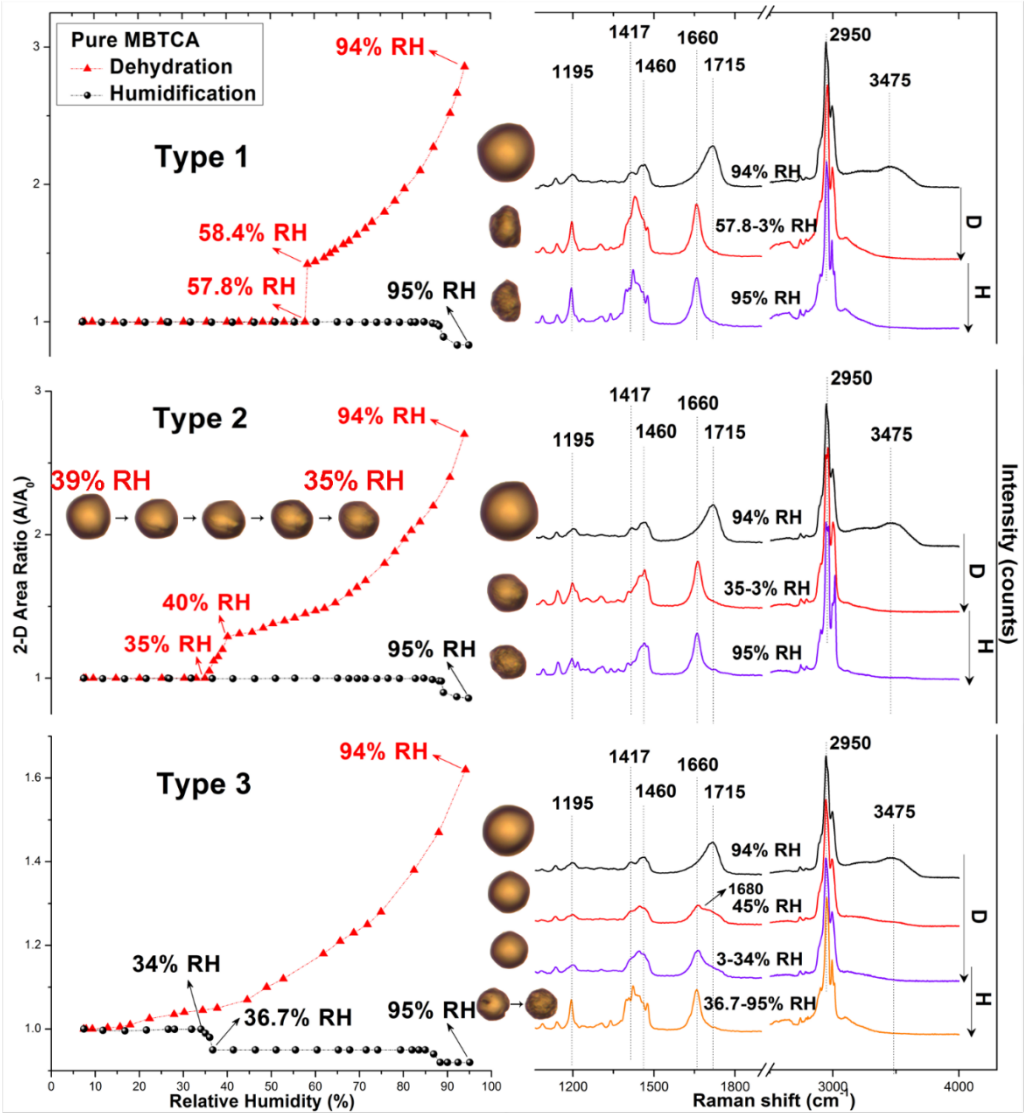

Figure 3. Hygroscopic curves, corresponding optical images, and Raman spectra at specific RHs of (a) mono-, (b) di-, and (c) tri-sodium MBTCA salt aerosols. The recorded transition RHs during the dehydration and humidification processes are marked with arrows in the hygroscopic curves.

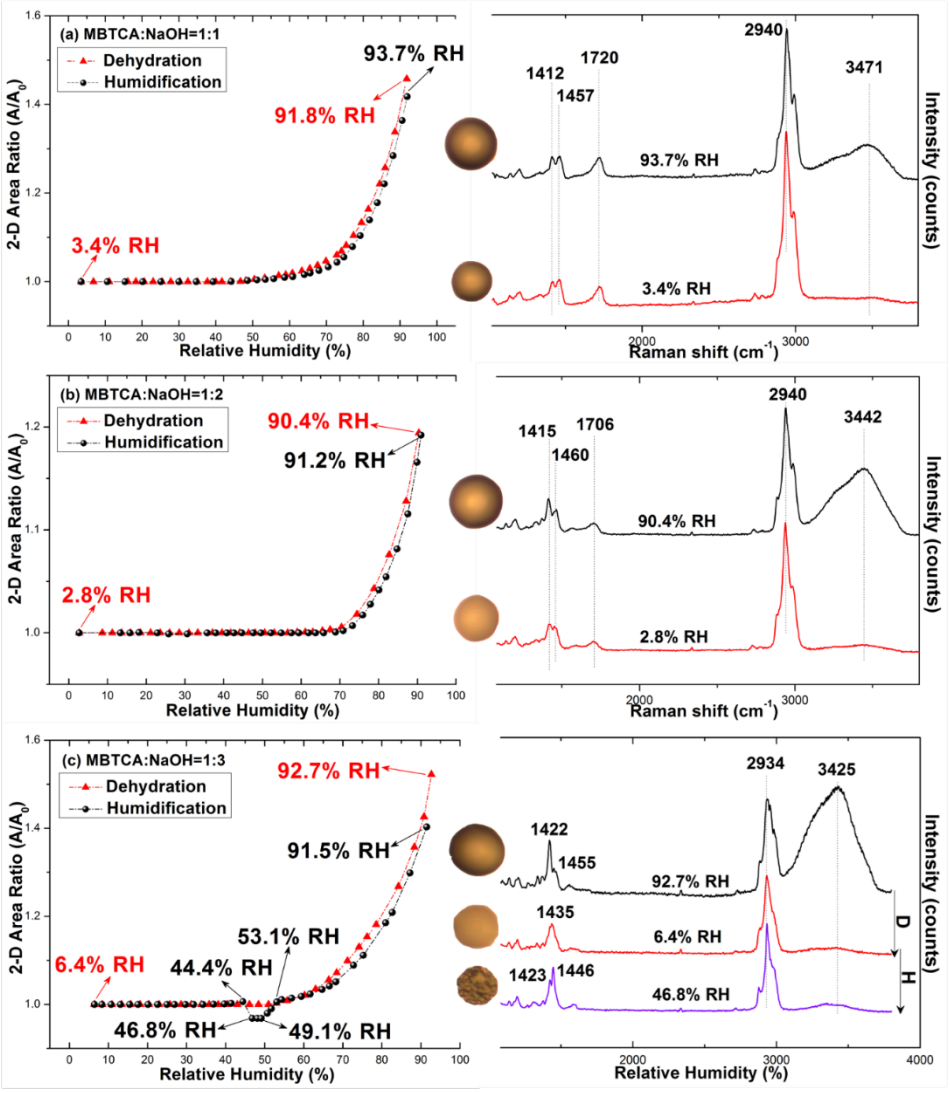

Figure 4. Hygroscopic curves, corresponding optical images, and Raman spectra at specific RHs of MBTCA:NaCl = (a) 1:1 and (b) 2:1. The recorded transition RHs during the dehydration (D) and humidification (H) processes and the chemical compositions of the mixtures at certain RHs are marked with arrows in the hygroscopic curves. The phase notations shown in parenthesis are s=solid; aq=aqueous; and as=amorphous solid.

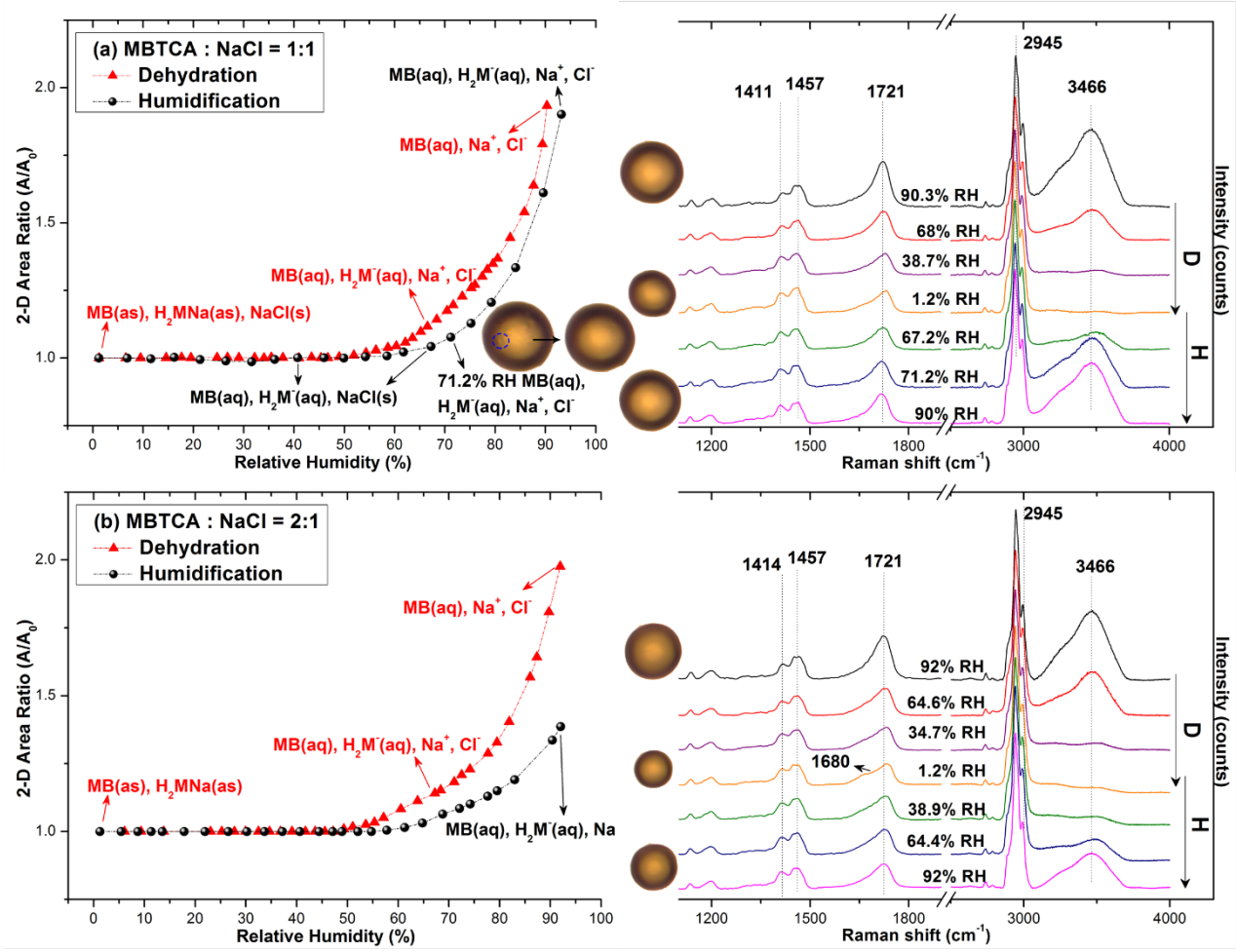

Figure 5. Hygroscopic curves, corresponding optical images, and Raman spectra at specific RHs of MBTCA:NaCl = (a) 1:2 and (b) 1:3. The recorded transition RHs during the dehydration (D) and humidification (H) processes and the chemical compositions of the mixtures at certain RHs are marked with arrows in the hygroscopic curves. The phase notations shown in parenthesis are s=solid; aq=aqueous; and as=amorphous solid.

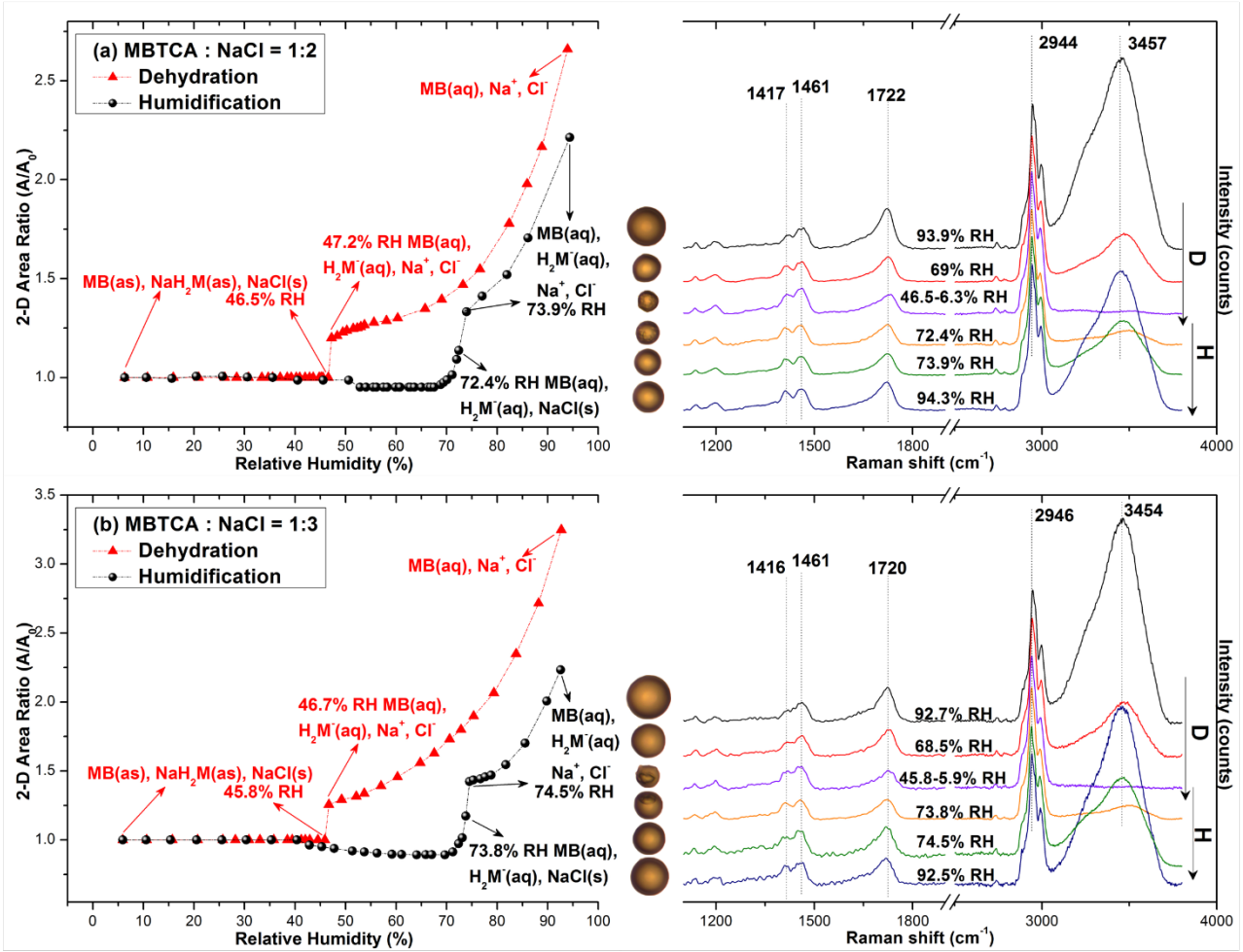

Figure 6. (a) Raman spectra of pure $NaH_2M$ and mixture aerosols with mixing ratios of MBTCA:NaCl = 1:1, 1:2, and 1:3 obtained at the end of the humidification process, which were normalized to the $CH_3$ peak at 1458 $cm^{-1}$ and (b) Raman spectra of pure MBTCA, mixture of MBTCA:$NaH_2M$ = 1:1, and pure $NaH_2M$, which are normalized to the $CH_3$ peak at 1460 $cm^{-1}$.

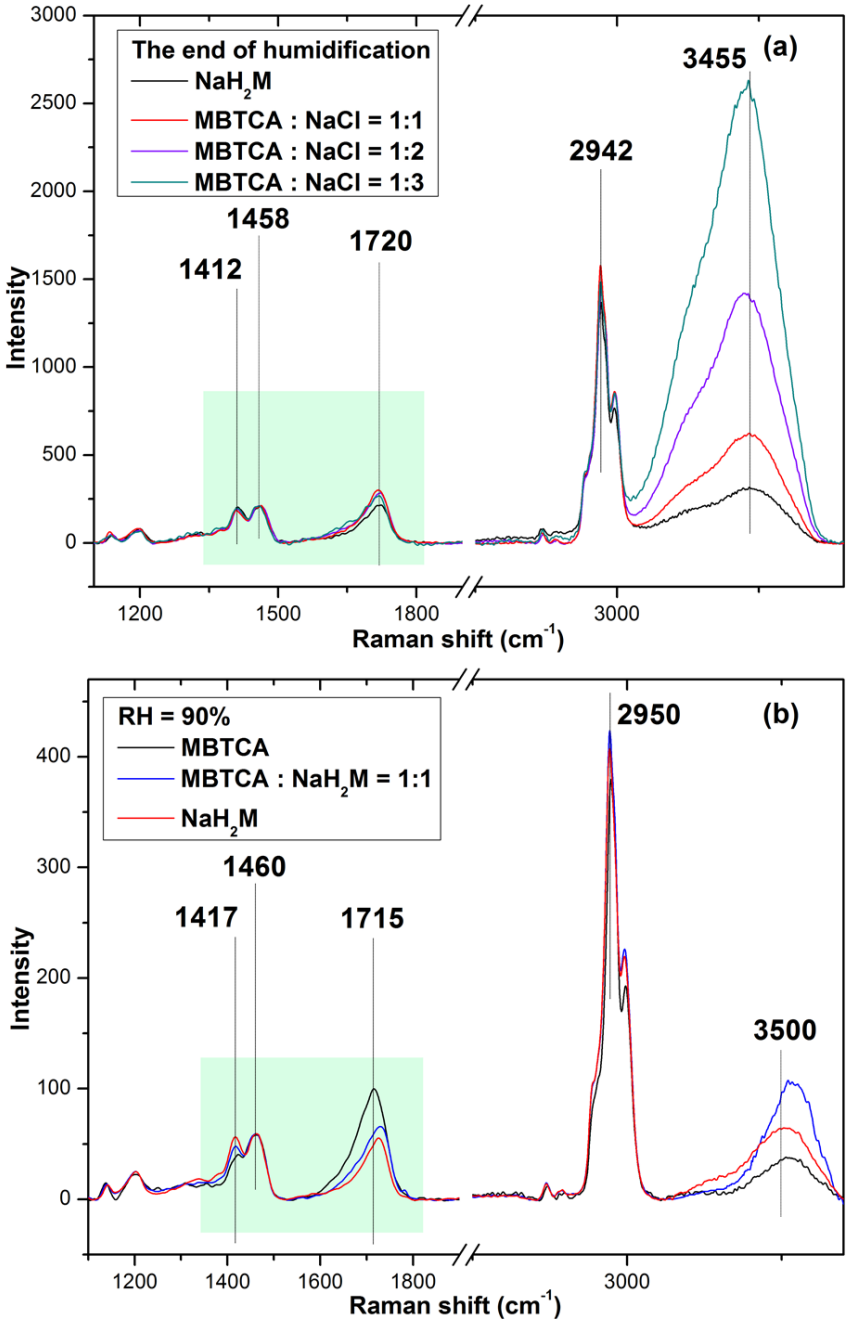

Figure 7. (a) Calibration curve calculated from the intensity ratios of two peaks at 1460 and 1720 $cm^{-1}$ as a function of RH for $NaH_2M$, MBTCA:$NaH_2M$ = 1:1, and MBTCA aerosols; (b) chemical reactivity represented as the degree of reaction for mixture aerosols of MBTCA:NaCl = 1:1, 1:2, 1:3, and 2:1 during the dehydration and humidification processes.

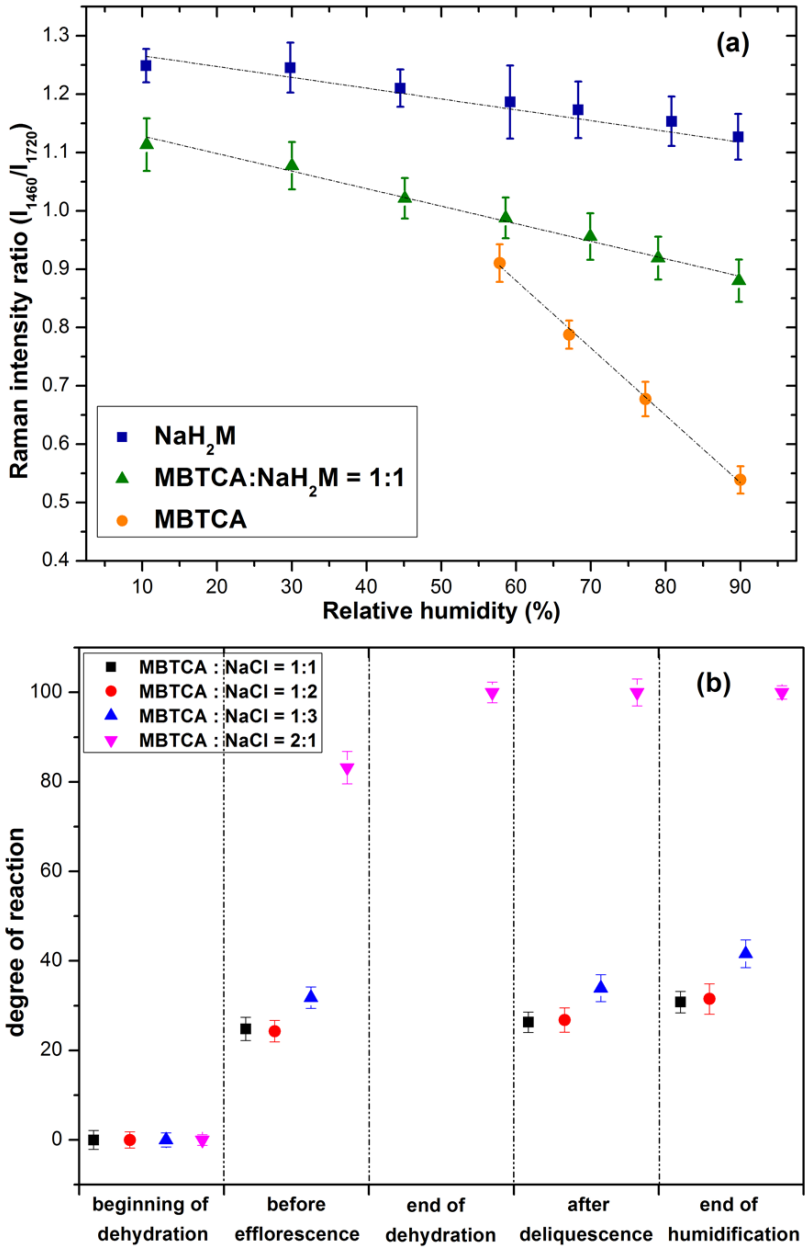

Figure 8. (a) Secondary electron images (SEIs) and elemental X-ray maps for C (from MBTCA and $NaH_2M$), Na (from $NaH_2M$ and NaCl), and Cl (from NaCl). The scale bars are for 5 μm; (b) X-ray spectra and elemental concentrations of particles with four mixing ratios.

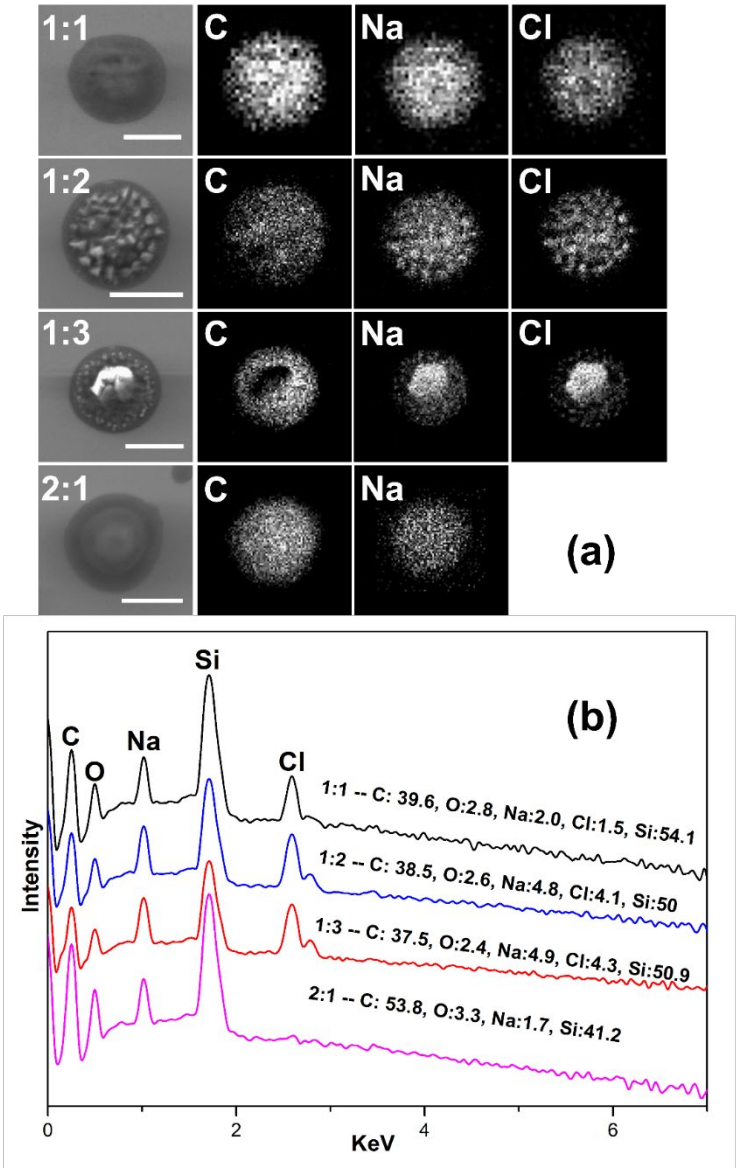

Figure 9. Hygroscopic curves, corresponding optical images, and Raman spectra at specific RHs of MBTCA:NaCl = (a) 1:1, (b) 1:2, and (c) 1:3 mixture particles in the levitation system. The recorded transition RHs during the humidification (H) and dehydration (D) processes and the chemical compositions of the mixtures at certain RHs are marked with arrows in the hygroscopic curves. The phase notations shown in parenthesis are s=solid; aq=aqueous; and as=amorphous solid.